Heliyon 10 (2024) e38432

Contents lists available at ScienceDirect

Heliyon

journal homepage: www.cell.com/heliyon

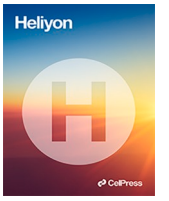

Research article

A comprehensive investigation of the nano-[Cu_2-$(DIP)_2$-EA] effects on HSA through spectroscopic procedures and computer simulations

Nahid Shahabadi *, Lida Ghaffari

Department of Inorganic Chemistry, Faculty of Chemistry, Razi University, Kermanshah, Iran

ARTICLE INFO

Keywords:
HSA interaction
Nano-binuclear Cu(II) complex
Multi-spectroscopic approach
Fluorescence quenching
Sudlow's site I/IIA
Molecular docking modeling

ABSTRACT

In this research, the toxicity of nano-[Cu_2-$(DIP)_2$-EA], a metal nano-complex consisting of ellagic acid and bathophenanthroline ligands, on human serum albumin (HSA) at a protein level was investigated. Molecular docking simulations and spectral analyses were conducted in a simulated physiological environment at pH 7.4 to explore the interaction of nano-[Cu_2-$(DIP)_2$-EA] with HSA. The results represented an increase in albumin absorption upon exposure to nano-[Cu_2-$(DIP)_2$-EA], demonstrating significant interaction between the two compounds. Steady-state and time-resolved fluorescence measurements pointed out that nano-[Cu_2-$(DIP)_2$-EA] induced static quenching of the albumin's intrinsic fluorescence with a high binding affinity of approximately 10^6 mol/L in a 1:1 interaction ratio. The thermodynamic variables clarified that binding of nano-[Cu_2-$(DIP)_2$-EA] to albumin occurs spontaneously and primarily driven by van der Waals interactions and H-bonds. The results of the computer simulations and the binding displacement experiments utilizing the site markers warfarin and ibuprofen revealed that nano-[Cu_2-$(DIP)_2$-EA] binds to site I within the subdomain IIA of albumin. Circular dichroism analysis elaborated that nano-[Cu_2-$(DIP)_2$-EA] slightly perturbed the microenvironment around of tryptophan residues and diminished the α-helix structure stability to a negligible amount.

1. Introduction

An understanding of the pharmacokinetics of drugs, such as their transport in plasma and delivery to target sites, is essential for deciphering a drug's functionality within biological systems. After administration, medications circulate through the bloodstream, with their initial interaction occurring at the level of plasma proteins. The circulatory system contains a diverse array of proteins and peptides, with human serum albumin (HSA) being the predominant protein, comprising over 50 % of plasma proteins. Other significant plasma proteins exist at much lower concentrations. While various essential transporter proteins are present in the human body, HSA primarily facilitates drug-protein interactions. This heart-shaped protein, characterized by X-ray crystallography, consists of 585 amino acids (66.5 kDa) arranged in a single-stranded α-helical configuration. Its structure includes three domains, each divided into two subdomains designated as A and B. Notably, areas IIA and IIIA—termed Sudlow's site I and site II, respectively—are located within these subdomains. As a versatile carrier, HSA possesses multiple binding sites that accommodate a wide variety of ligands including drugs, fatty acids, metal ions, amino acids, vitamins, hormones, and water. The functions of anticancer drugs can vary significantly.

* Corresponding author.
E-mail addresses: n.shahabadi@razi.ac.ir (N. Shahabadi), l.ghaffari@razi.ac.ir (L. Ghaffari).

https://doi.org/10.1016/j.heliyon.2024.e38432
Received 14 June 2024; Received in revised form 17 September 2024; Accepted 24 September 2024
Available online 25 September 2024

HSA may influence the concentration of free, biologically active components of these drugs through interaction. Strong binding of drugs to HSA can reduce the concentration of unbound drugs in plasma, whereas weak binding may result in shortened drug lifespan or inadequate distribution. Hence, identifying the binding sites of drugs within HSA enhances our awareness of anticancer drugs competing with other compounds at these sites [1–5].

Coordination compounds are considerable in chemistry due to their unique structural arrangements and extensive applications across various fields. While not a novel concept in medicine and drug discovery, they often receive insufficient attention from medicinal chemists. These compounds not only possess biological relevance but also encompass a range of drug-like molecules and pharmaceuticals [6]. The quest for innovative metal-containing complexes with therapeutic potential has inspired researchers to explore, synthesize, and characterize metal-based complexes for medicinal uses. Central to this exploration is the grasp of binding mechanisms between biological targets and metallic complexes [7]. Modifying the nature of ligands and donor atoms can refine the pharmacological properties of metal complexes [8]. For instance, platinum complexes are recognized as effective anticancer drugs [6]; however, their clinical application is often hindered by severe side effects, including nephrotoxicity, neurotoxicity, and ototoxicity. As a result, the development of new copper coordination compounds exhibiting anticancer activity is an evolving and promising field in medicinal chemistry [8]. Copper plays a crucial role in the formation and function of several enzymes and proteins. Complexes enhanced with copper are highly valued due to the redox activity and biogenicity of copper ions, which facilitate a multitude of cellular pathways. Copper complexes serve as effective antitumor agents, presenting a cost-effective and safer alternative to traditional platinum-based chemotherapy. Furthermore, the redox activity of these copper-based compounds extends their therapeutic potential beyond merely antiproliferative effects; they can also effectively combat viral and microbial infections, as well as inflammatory conditions, through various mechanisms of action. The advancement of delivery and controlled release systems for copper complexes exemplifies their success in clinical applications [8].

The choice of coordinating ligands profoundly impacts both the toxicity and mechanism of action in cancer treatment [9]. Ligand selection is vital in determining the biological activity of metal complexes [10], as specific ligands can modulate the adverse effects associated with excess metal ions. When ligands coordinate with metal ions, substantial alterations occur, such as increases in lipophilicity, stabilization of distinct oxidation states, and enhanced substitution stability [11]. Bathophenanthroline, with its chelating mode of coordination, is a versatile ligand that has been employed to create numerous structures across various dimensionalities [12]. Given that HSA can interact with lipophilic compounds and transport a diverse array of hydrophobic ligands [1,3], we utilized 4, 7-diphenyl-1,10-phenanthroline (bathophenanthroline) in the current investigation as both an auxiliary and ancillary ligand for the synthesis of nano-[Cu_2-$(DIP)_2$-EA].

In recent decades, nanomaterials and nanotechnology have garnered substantial interest in research due to their remarkable physical, chemical, and biological attributes. Previous investigations have indicated that interactions between biomolecules and nanomaterials can alter biomolecular structures, disrupting the normal functions of proteins, which may result in undesirable biological reactions and toxicity. The size of nano-metal complexes is believed to influence their bioactivity, underscoring the importance of comprehension these interactions [13–18].

Extensive studies have established that ellagic acid (EA), a polyphenolic compound found in dicotyledonous plants, exhibits potent anti-inflammatory, antimutagenic, antiproliferative, and antioxidant properties. This compound is prevalent in various fruits and nuts and is primarily generated in plants through the hydrolysis of ellagitannins, a widespread class of secondary metabolites. EA demonstrates a variety of beneficial effects, including neuroprotective, hepatoprotective, cardioprotective, antiallergic, antinociceptive, antiestrogenic, skin-protecting, wound-healing, osteogenic, antimicrobial, antiviral, and antiparasitic activities, making it promising for cancer prevention and treatment. Moreover, EA has shown protective effects against the toxicity of metals, metalloids, and natural toxins, and it is utilized in both the pharmaceutical and cosmetics industries. Oxidative stress, resulting from excessive production of reactive oxygen and nitrogen species, is implicated in a range of human diseases. Natural polyphenols like ellagic acid possess multitargeting capabilities to mitigate oxidative stress, positioning them as advantageous therapeutic agents [19–23].

Spectroscopic techniques provide crucial perspectives on the binding characteristics and specific binding sites within macromolecules. These approaches are increasingly favored over traditional methods due to their simplicity, speed, and reproducibility [7].

This study focuses on the nano-material [Cu_2-$(DIP)_2$-EA], which consists of aggregated components, aiming to enhance our apprehension of its interactions with biological molecules, particularly HSA. We employ multispectral and computational methods as a lucrative toolkit for investigating the nano-[Cu_2-$(DIP)_2$-EA]-HSA interactions. The study evaluates agents affecting binding affinity and fluorescence quenching techniques that play a role in predicting the mechanism and evaluating the interactions engaged. Thus, we build upon our previous research [24] to explore the binding interactions between nano-[Cu_2-$(DIP)_2$-EA] and HSA. Utilizing both experimental and theoretical methods, our goal is to gain insights into the interaction mechanisms of metal nano-complexes with HSA. We believe that the from this research could markedly enhance our knowledge about how these complexes findings interact with the protein, paving the way for the development of more effective pharmaceutical agents, particularly in the treatment of cancer and other human diseases.

2. Experimental section

2.1. Compounds and solutions

Not refined, all of the materials employed in the work had the quality of analytical reagents. Additionally, the stock solutions in net aqueous media were made in a buffer solution that had 0.1 M phosphate buffer added to bring the pH down to 7.4. The phosphate buffer solution (0.1 M) was procured from Na_2HPO_4 and NaH_2PO_4 salts at ambient temperature. To prepare the HSA stock solution,

0.0132 g of HSA crystals were added to 2 mL of phosphate buffer without stirring the solution or shaking the container; the container was then placed in the dark at 4 °C for 1 h, resulting in a final concentration of 1.00×10^{-4} M. Moreover, the stock solutions of warfarin, ibuprofen, and nano-[Cu_2-$(DIP)_2$-EA were 1.00×10^{-3} M.

2.2. Synthesis of nano-[Cu_2-$(DIP)_2$-EA

The following synthesis approach was utilized by Shahabadi and co-workers [24] to create the nano-[Cu_2-$(DIP)_2$-EA (Fig. 1). In short, 35 ml of ethanol solvent, which had been previously alkalinized to pH 8.8, was used to dissolve 0.1511 g (0.5 mmol) of ellagic acid x.H_2O and 0.3324 g (1 mmol) of bathophenanthroline separately. Subsequently, the two solutions were combined and mixed together to undergo reflux. Next, 0.2416 g (1 mmol) of $Cu(NO_3)_2.3H_2O$ was dissolved into 10 ml of this solvent. Over the course of 2 h, the copper nitrate salt solution got added to the solution dropwise while reflux was occurring. After 24 h, the reflux process was halted and the reaction mixture was centrifuged at ambient temperature at 3800 rpm for 10 min. The formed blackish solid was filtered off, rinsed with an ethanol and water mixture, and allowed to dry for 24 h at 50 °C in an oven. Yield: 0.34 g, 62 %. Anal. M.p: 248–250 °C; IR (KBr, cm^{-1}): 3418 (ν O-H), 2920 (ν C-H), 1714 (ν C=O), 1615 (ν C=N), 1566 (ν C=C), 1272 (ν C-O), 768 (ν C-H), 549 (ν Cu-N), 482 (ν Cu-O). MS: $m/z = 1090$ $[M]^+$. UV–vis: λ_{max} (nano-[Cu_2-$(DIP)_2$-EA) = 289 nm; λ_{max} (bathophenanthroline) = 285 nm; λ_{max} (ellagic acid) = 324 nm. λ_{max} ($Cu(NO_3)_2.3H_2O$) = -.

2.3. UV–vis spectrophotometry

A NordantecT-80 UV–Vis spectrophotometer model was served to detect the UV–Vis absorption data in the wavelength span of 240 nm–350 nm utilizing a 1.0 cm cell. In UV–Vis titration tests, the concentration of HSA was held steady at 9.6×10^{-7} M while the concentration of nano-[Cu_2-$(DIP)_2$-EA differed from 0.0 to 4.8×10^{-7} to 7.4×10^{-6} (ri = [complex]/[HSA] = 0.0 to 7.7). Shortly after

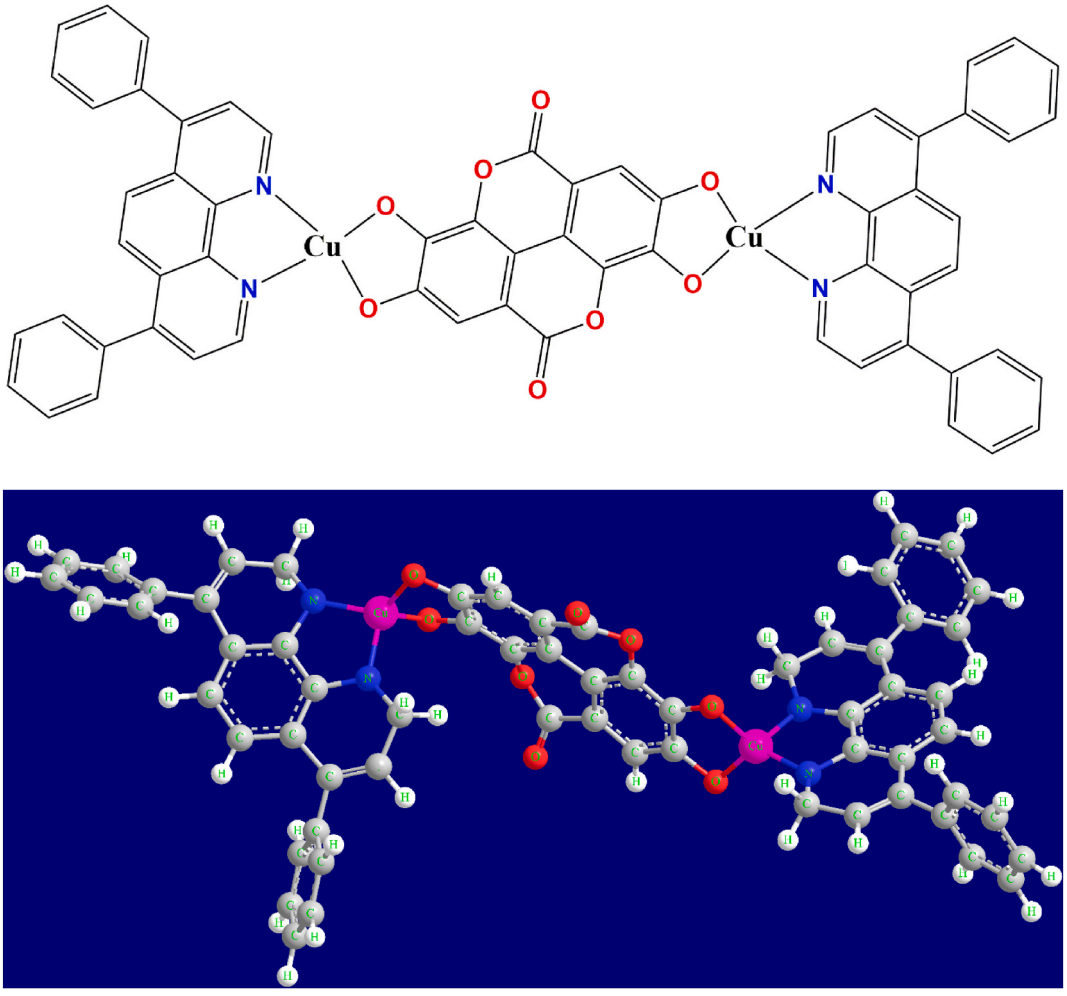

Fig. 1. The computed structure of the nano-material [Cu_2-$(DIP)_2$-EA].

adding the nano-[Cu_2-$(DIP)_2$-EA solution and reaching equilibrium, the absorbance amounts were noted.

In order to omit the effect of the nano-[Cu_2-$(DIP)_2$-EA absorption, control tests were conducted using a series of identical small fractions of the corresponding nano-[Cu_2-$(DIP)_2$-EA stock solutions in the absence of albumin as reference solutions. Interaction spectra were then obtained by subtracting the spectra of the nano-[Cu_2-$(DIP)_2$-EA reference solutions from the corresponding full spectra [25,26].

2.4. Fluorescence measurements

For fluorescence analysis, a JASCO FP 6200 spectrofluorimeter featuring a thermostatic bath and 1 cm quartz cell was put to use. The fluorescence quenching experiments were conducted at $\lambda_{ex} = 295$ nm. Adjustments were made to the emission and excitation bandwidths at 5 and 10, respectively. For the HSA, the highest emission of fluorescence was detected at 347 nm. We acquired the fluorescence spectra with a wavelength area of 300–450 nm at 289, 292, and 295, 297 K. The ensuing steps were taken to carry out the nano-[Cu_2-$(DIP)_2$-EA-HSA interactions: a specific amount of HSA (2.9×10^{-6} M) was titrated through enhancing the amount of nano-[Cu_2-$(DIP)_2$-EA (from 0.0, 2.5×10^{-7} to 2.5×10^{-6} M). Time-resolved fluorescence decays were conducted for HSA solution (2.9×10^{-6} M) without and with the various concentrations of nano-[Cu_2-$(DIP)_2$-EA (from 0.0, 2.5×10^{-7} to 2.5×10^{-6} M) to validate the main fluorescence quenching mechanism. The measurements were performed in triplicate at room temperature with excitation at 282 nm [25], and emission wavelength at 338 nm [26], response time: 01 s, data pitch: 0.5 s, and time measurement duration: 300 s [27].

Displacement evaluations at 298 K through site markers of warfarin and ibuprofen were performed at fixed markers levels of 2.8×10^{-5} M and the protein at 2.9×10^{-6} M, respectively. The binding constant for the nano-[Cu_2-$(DIP)_2$-EA-HSA was determined by means of fluorescence quenching titration with the specific site markers at varying concentrations of nano-[Cu_2-$(DIP)_2$-EA (ranging from 0.00, 4.71×10^{-7} to 8.22×10^{-5} M). The emission wavelength was set within the 300–500 nm scope, with an excitation wavelength of 295 nm, all conducted at ambient temp. The correction of fluorescence intensities was executed taking into account the absorption of the exciting light beam and the re-absorption of the emitted light beam via the compound structure at the excitation or emission wavelength, as determined by a specific equation (Eq. (1)) [28]:

$$F_{cor} = F_{obs} \times exp\left(\frac{A_{ex} + A_{em}}{2}\right) \quad (1)$$

Wherein, the modified and observed fluorescence intensities are denoted as F_{cor} and F_{obs}, correspondingly, while A_{ex} and A_{em} symbolize the absorbance measurements of nano-[Cu_2-$(DIP)_2$-EA at the excitation and emission wavelengths, respectively.

Subsequently, the modified quantities were exerted to elucidate the quenching process of the nano-[Cu_2-$(DIP)_2$-EA-HSA by employing the Stern-Volmer's formula (Eq. (2)) [29,30]:

$$F_o / F = 1 + K_{SV}[Q] = 1 + K_q \tau_0 [Q] \quad (2)$$

Here, the indexes F_0 and F illustrate the intensity of fluorescence prior to and following the quencher addition, respectively. The quenching constant (K_{SV}) came by the linear plot's slope of F_0/F versus [Q]. The quenching rate constant of a biomolecule and the average lifetime of the fluorophore in the non-presence of the quencher are indicated via K_q and $\tau_o = 10^{-8}$ s, respectively. Eventually, the quencher concentration is exhibited via [Q].

The number of binding sites and the binding constant in the nano-[Cu_2-$(DIP)_2$-EA-HSA were gained through the formula (Eq. (3)):

$$log\frac{F_0 - F}{F} = log K_b + nlog[Q] \quad (3)$$

The formula describes the fluorescence intensities of the fluoroph ore in the attendance and non-attendance of the quencher quantities as F_0 and F, respectively [31].

The Van't Hoff formula (Eq. (4)) was exerted for calculating the thermodynamic values ΔH and ΔS [32]:

$$ln K_b = -\Delta H/_{RT} + \Delta S/_{R} \quad (4)$$

In the given formula, the universal gas constant, temperature in Kelvin, and the binding constant at that temperature are clarified applying the symbols R, T, and K_b, respectively. Ultimately, Gibbs free energy change (ΔG) was captured through the Gibbs-Helmholtz's formula (Eq. (5)) [33]:

$$\Delta G = -RTlnK_b \quad (5)$$

In the time-resolved fluorescence analysis, the lifetime τ was determined [34] by fitting the fluorescence intensity I as a function of the delay time t (nanosecond) employing the following equation (Eq. (6)), with I_0 representing the initial intensity at t = 0:

$$I(\lambda) = I_0(\lambda) \times e^{-t/\tau} \quad (6)$$

The dynamic component of the observed quenching was assessed [35,36] through lifetime measurements, applying the equation (Eq. (7)):

$$\frac{\tau_0}{\tau} = 1 + K_D\,[Q] \tag{7}$$

Here, τ_0 and τ represent the fluorescence lifetimes of HSA in the absence and presence of nano-[Cu_2-$(DIP)_2$-EA, respectively, while K_D signifies the dynamic quenching constant.

The static quenching constant (K_S) was calculated [25,35,36] using equation (Eq. (8)), which involves plotting the relationship between K_{app} and the concentration of [Q], incorporating the value of K_D obtained from the lifetime measurements:

$$K_{app} = \frac{F_0 - F/F}{[Q]} = K_S + K_D + (K_S K_D [Q]) \tag{8}$$

In this equation, F_0 and F correspond to the steady-state fluorescence intensities of HSA without and with the addition of nano-[Cu_2-$(DIP)_2$-EA, respectively. The terms K_{app}, [Q], K_D, and K_S represent the apparent quenching constant, the concentration of nano-[Cu_2-$(DIP)_2$-EA, the dynamic quenching constant, and the static quenching constant, respectively.

In the Job plot, the fluorescence bands of several solutions were recorded between 300 and 450 nm wavelengths, with an excitation wavelength of 295 nm at 298 K; the concentrations of HSA and nano-[Cu_2-$(DIP)_2$-EA were varied while the overall concentration was kept constant (5.0×10^{-6} M). The binding stoichiometry was got from the formula (Eq. (9)) [37]:

$$binding\ stoichiometry = \frac{1 - \chi_{\text{ nano-[Cu2-(DIP)2-EA}}}{\chi_{\text{ nano-[Cu2-(DIP)2-EA}}} \tag{9}$$

In the aforementioned formula, the mole fraction of nano-[Cu_2-$(DIP)_2$-EA is symbolized by $\chi_{\text{ nano-[Cu2-(DIP)2-EA}}$.

2.5. CD spectroscopy

A JASCO spectropolarimeter Model J-810 (Tokyo, Japan) was implemented to collect the CD data of the protein (4.97×10^{-7} M) in the existence of nano-[Cu_2-$(DIP)_2$-EA (0.00, 2.48, 4.95, and 7.41×10^{-9} M) through a quartz cell that measured 1 cm. The spectra were taken between 200 nm and 250 nm in wavelength range, at 25 °C. Equation (Eq. (10)) went to use to convert the raw spectra data to mean residual ellipticity [θ] (deg cm^2 $dmol^{-1}$) namely concentration independent parameter:

$$MRE = \frac{\Theta\lambda.M}{(10.C.l)} \tag{10}$$

In which, C is the HSA concentration in mg ml^{-1}, l is the cell's path-length in centimeters, Θλ is the seen ellipticity in millidegrees at wavelength λ, and M is the mean residue weight of HSA. The α-helix content percentage of HSA was determined based on the ellipticity quantities at 208 nm from the equation below (Eq. (11)) [38]:

$$\alpha helix\ (\%) = \frac{(-MRE_{208} - 4000)}{(33000 - 4000)} \times 100 \tag{11}$$

2.6. Molecular docking

For the docking process, the Auto Dock Vina (version 1.1.2, MGL tools 1.5.6) was launched. The crystalline form of the protein was earn from the Protein Data Bank (PDB ID: 7VR0) [39]. The files of ligand (nano-[Cu_2-$(DIP)_2$-EA) and receptor (HSA) were procured by Auto Dock Tools. (x min: 12.8439 x max: 29.2147), (y min: 3.16208 y max: 35.3773) and (z min: 10.6771 z max: 28.4299) (grid = 1.00 °A) were the settings for the grid box. The Lamarckian genetic algorithm was run to make the docking definitions. The remaining factors were set to their default settings. BIOVIA Discovery Studio Visualizer 2021 was exploited to visualize the docked poses [40].

2.7. Statistical analysis

2.7.1. UV–vis spectrophotometry

In the UV–Vis titration experiments, absorption data were collected within the wavelength range of 240 nm–350 nm using a Nordantec T-80 UV–Vis spectrophotometer. Different concentrations of nano-[Cu_2-$(DIP)_2$-EA] were tested in the presence of a constant concentration of HSA. Specifically, UV–Vis spectrophotometry was employed to detect the absorption characteristics of the system, with absorbance values measured after the addition of the nano-[Cu_2-$(DIP)_2$-EA] solution and the establishment of equilibrium.

2.7.2. Fluorescence spectroscopy

Fluorescence quenching experiments were conducted using a JASCO FP 6200 spectrofluorimeter, measuring emission spectra at various temperatures and concentrations of nano-[Cu_2-$(DIP)_2$-EA] and HSA. These experiments involved multiple calculations and evaluations to determine parameters such as binding constants, quenching constants, and thermodynamic values. Key equations employed included the Stern-Volmer equation for quenching analysis, equations for determining the number of binding sites and binding constants, the Van't Hoff equation for thermodynamic parameters, and the Gibbs-Helmholtz equation for calculating Gibbs

free energy changes. Additionally, Job plot analysis was performed to assess binding stoichiometry.

2.7.3. Circular dichroism (CD) Spectropolarimetry

CD data for HSA in the presence of nano-[Cu_2-$(DIP)_2$-EA] were collected using a JASCO spectropolarimeter, analyzing spectra within a specified wavelength range. The analysis of CD data involved converting raw spectral data to mean residual ellipticity [θ] using equation (Eq. (7)). This parameter was employed to calculate the percentage of α-helix content of HSA based on equation (Eq. (8)), specifically at 208 nm. The interpretation of the CD data provided knowledge about the secondary structure content of the protein in the presence of varying concentrations of nano-[Cu_2-$(DIP)_2$-EA].

2.7.4. Molecular docking

Molecular docking simulations were executed using Auto Dock Vina to analyze the binding interaction between nano-[Cu_2-$(DIP)_2$-EA] and HSA. Molecular docking provided crucial cognition of the potential binding orientations and affinities of the ligand towards the protein receptor, aiding in understanding the molecular interactions at a structural level.

In the molecular docking process, the following steps and tools were utilized.

a) **Software and Tools:** Molecular docking simulations were conducted using AutoDock Vina (version 1.1.2) in conjunction with MGL Tools (version 1.5.6). These tools enable the prediction of binding modes and affinities between the ligand (nano-[Cu_2-$(DIP)_2$-EA]) and the receptor (HSA).
b) **Protein Structure:** The crystalline structure of HSA was obtained from the Protein Data Bank (PDB ID: 7VR0), serving as the receptor for the docking studies and yielding significant perspectives on the binding interactions. **Preparation of Ligand and Receptor:** The ligand (nano-[Cu_2-$(DIP)_2$-EA]) and receptor (HSA) files were prepared using AutoDock Tools, ensuring that they contained the necessary information and coordinates required for the docking simulations.
c) **Grid Box Settings:** A grid box was defined for the docking simulations with specific dimensions and coordinates: x min: 12.8439, x max: 29.2147, y min: 3.16208, y max: 35.3773, z min: 10.6771, z max: 28.4299. The grid spacing was set to 1.00 Å, influencing the search space for the ligand within the receptor's binding site.
d) **Docking Algorithm:** The Lamarckian genetic algorithm was employed to perform the docking calculations, aiding in the exploration of conformational space and predicting the optimal binding pose of the ligand within the receptor's binding site.
e) **Visualization:** The results of the docking simulations, including the docked poses of the ligand within the receptor, were visualized using BIOVIA Discovery Studio Visualizer 2021. This software facilitates interactive visualization and analysis of molecular structures and their interactions.

2.8. Rationale for selecting specific tests

2.8.1. UV–vis spectrophotometry

UV–Vis spectrophotometry is a widely employed technique for determining the absorption characteristics of compounds in solution at specific wavelengths. This method is particularly suitable for studying the interactions between biomacromolecules, such as HSA, and coordination compounds, exemplified here by nano-[Cu_2-$(DIP)_2$-EA].

2.8.2. Fluorescence spectroscopy

The selected tests and formulas were specifically chosen to assess the fluorescence quenching process associated with the interactions between nano-[Cu_2-$(DIP)_2$-EA] and HSA. This approach enables the determination of various parameters, including binding constants, quenching constants, thermodynamic values, and binding stoichiometry. These tests are standard in fluorescence analysis, offering critical information regarding molecular interactions and binding events.

2.8.3. Circular dichroism (CD) Spectropolarimetry

Circular Dichroism (CD) spectroscopy is a powerful technique for exploring the secondary structure of proteins and identifying conformational changes triggered by ligand binding. Hence, it was employed to analyze the CD data of HSA in the presence of varying concentrations of nano-[Cu_2-$(DIP)_2$-EA]. The specific wavelength range of 200 nm–250 nm was selected for measuring the CD spectra, as this range is particularly sensitive for analyzing protein secondary structures. Equation (Eq. (7)) was utilized to convert the raw CD spectral data to mean residual ellipticity, which facilitated the calculation of the percentage of α-helix content of the protein at 208 nm, as determined by equation (Eq. (8)).

2.8.4. Molecular docking

Molecular docking was performed using AutoDock Vina to study the interaction between the ligand (nano-[Cu_2-$(DIP)_2$-EA]) and the protein receptor (HSA). AutoDock Vina was chosen due to its effectiveness in predicting ligand-protein interactions and the availability of the crystalline structure of HSA from the Protein Data Bank (PDB ID: 7VR0).

2.9. Assumptions made and their testing

2.9.1. UV–vis spectrophotometry

i. Nano-[Cu_2-$(DIP)_2$-EA] interacts with HSA and binds to it.
ii. The UV–visible absorption profile of HSA, when interacting with other molecules, changes as a consequence of forming a complex with them.

Since the absorption spectroscopy in the UV–vis range is usually applied to study structural variations and the formation of new systems between biomacromolecules and other molecules, these assumptions were supported by the observed changes in the absorption spectra of HSA, including hyperchromism, following the gradual and sequential addition of nano-[Cu_2-$(DIP)_2$-EA] (see Fig. 2).

2.9.2. Fluorescence spectroscopy

i. The interaction between nano-[Cu_2-$(DIP)_2$-EA] and HSA is presumed to occur through either a static or dynamic quenching mechanism.

This assumption was supported by the observed decrease in fluorescence emission intensity with increasing concentrations of nano-[Cu_2-$(DIP)_2$-EA] (see Fig. 3A), as well as an analysis of the fluorescence quenching data (refer to Eq. (2), Fig. 4) and conclusions drawn from the experimental results (see Table 1).

ii. It is hypothesized that nano-[Cu_2-$(DIP)_2$-EA] interacts with HSA via the Sudlow binding sites.

This assumption is based on the results of binding studies and competitive emission experiments (see Figs. 8 and 9; Table 4). The use of specific binding site tracers, such as warfarin and ibuprofen, was employed to further investigate these binding interactions.

iii. Thermodynamic assessments can elucidate the forces involved in the protein-ligand interactions (HSA-nano-[Cu_2-$(DIP)_2$-EA]).

This assumption was validated by the observed decrease in fluorescence intensity with increasing concentrations of nano-[Cu_2-$(DIP)_2$-EA] (see Fig. 3A), and was further supported by an analysis of fluorescence quenching data (refer to Eqs. (3)–(5); Fig. 6) and

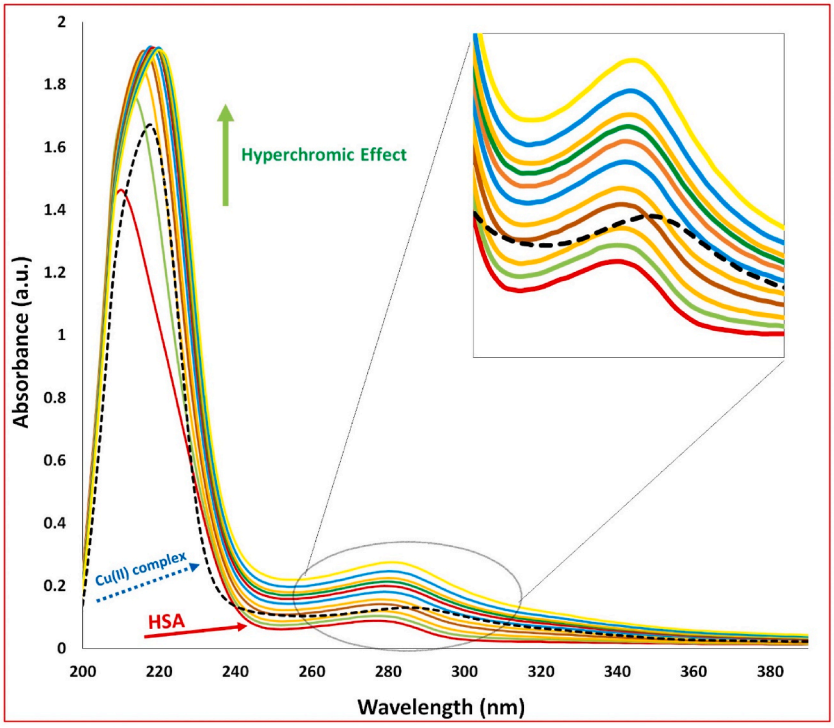

Fig. 2. The HSA (9.6×10^{-7} M) absorption spectra with and without nano-[Cu_2-$(DIP)_2$-EA]. The concentration of nano-[Cu_2-$(DIP)_2$-EA] ranges from 0.0, 4.8×10^{-7} to 7.4×10^{-6}; the punctulated black line displays absorption band of nano-[Cu_2-$(DIP)_2$-EA] (1.5×10^{-6} M) in phosphate buffer and pH 7.4 at 25 °C.

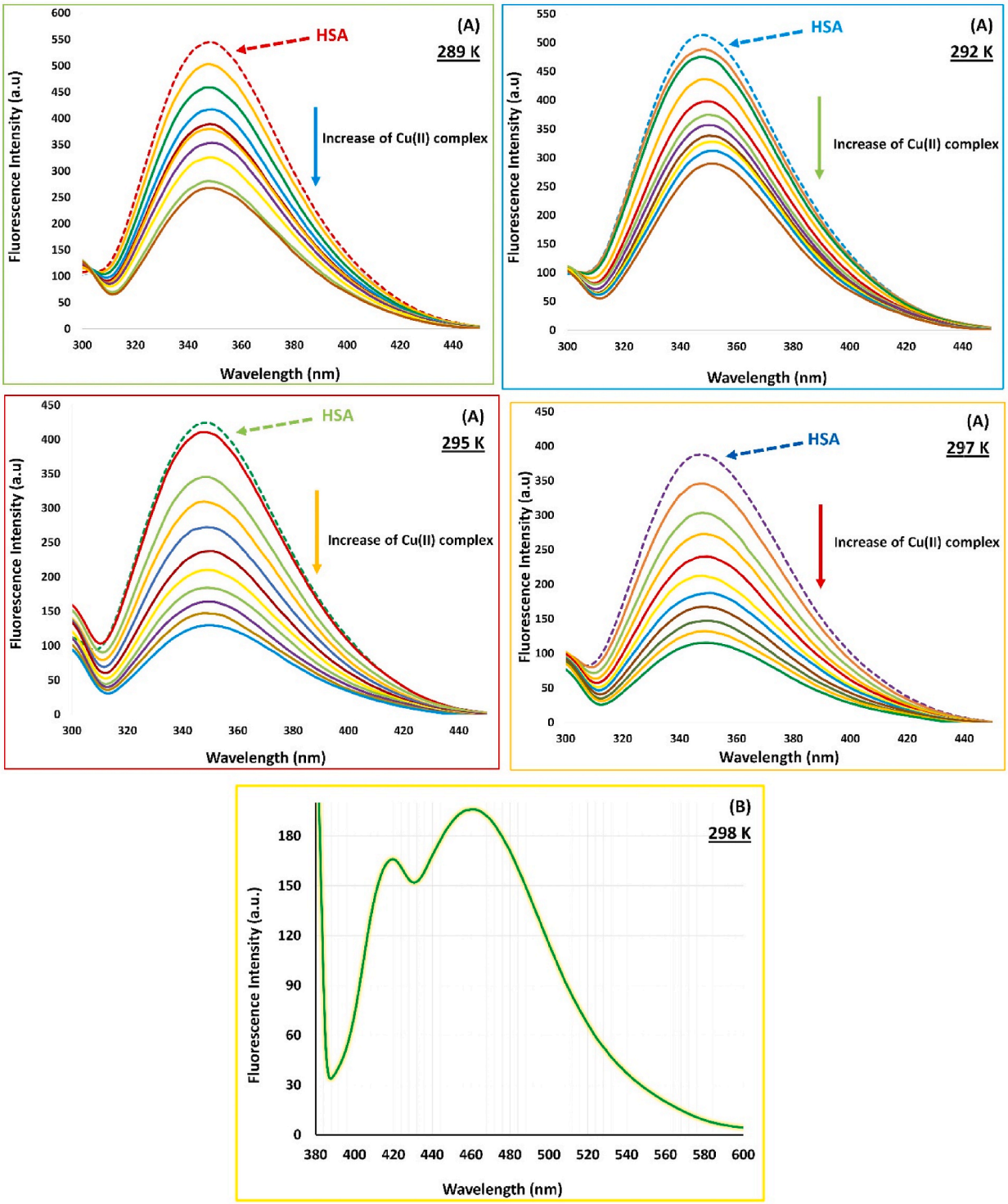

Fig. 3. A. Albumin (2.9×10^{-6} M) fluorescence spectra in phosphate buffer, at 289, 292, and 295, 297 K, in the non-existence and existence of nano-[Cu_2-$(DIP)_2$-EA] (0.0, 2.5×10^{-7} to 2.5×10^{-6} M) upon excitation at 295 nm; pH 7.4. **B)** The nano-[Cu_2-$(DIP)_2$-EA] (4.76×10^{-5} M) fluorescence spectrum in phosphate buffer at 25 °C and pH 7.4 following excitation at 363 nm.

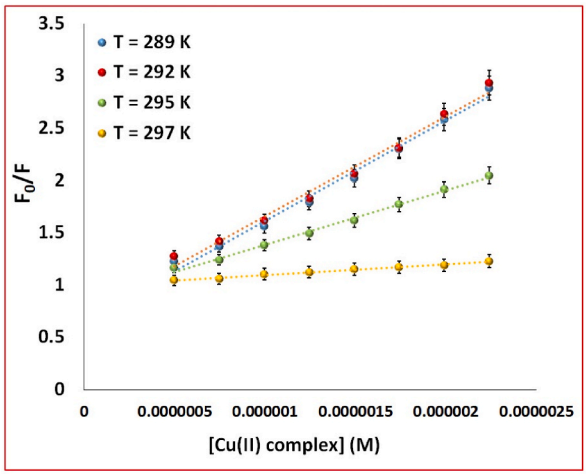

Fig. 4. The diagram of F_0/F vs. the nano-[Cu_2-$(DIP)_2$-EA] concentration to achieve the k_q amounts.

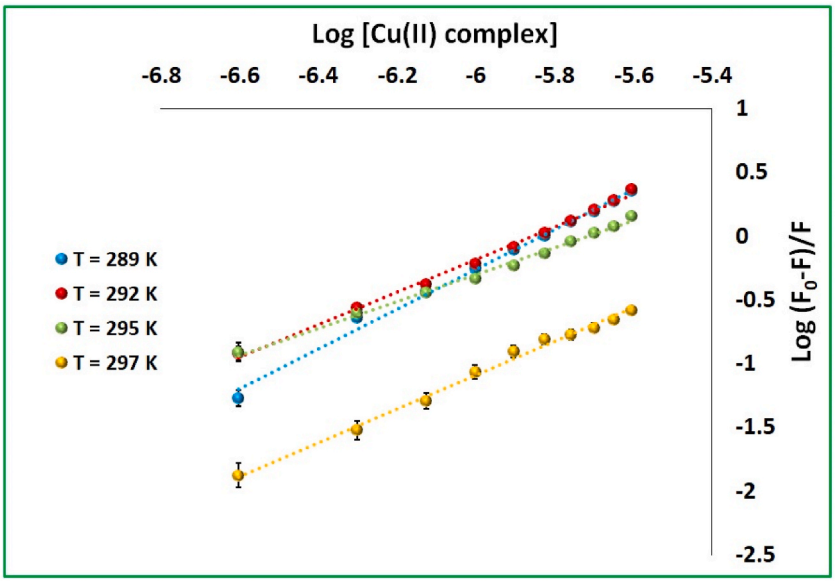

Fig. 5. The diagram of log $(F_0$-F)/F versus log [nano-[Cu_2-$(DIP)_2$-EA]] to gain the K_b amounts.

conclusions derived from the experimental results (see Table 3).

2.9.3. Circular dichroism (CD) Spectropolarimetry

It is assumed that the presence of nano-[Cu_2-$(DIP)_2$-EA] leads to alterations in the secondary structure of HSA, specifically affecting its α-helix content. This assumption was tested by comparing the CD spectra of HSA in the presence and absence of nano-[Cu_2-$(DIP)_2$-EA] (see Fig. 10). Calculations of mean residue ellipticity (MRE) at 208 nm (refer to Eq. (7)) and the percentage of α-helix content (refer to Eq. (8)) were conducted to assess any changes in secondary structure (see Table 5).

2.9.4. Molecular docking

The interaction mode of nano-[Cu_2-$(DIP)_2$-EA] with HSA is postulated to occur at the Sudlow I/IIA site, involving hydrogen bonding with specific amino acids. The assumptions regarding the interaction mode of nano-[Cu_2-$(DIP)_2$-EA] with HSA were substantiated through molecular docking simulations, which included visualization of interactions, utilization of scoring functions, and thermodynamic analyses. These testing methods validated the predicted binding mode and confirmed its alignment with experimental outcomes (see Figs. 11–13; Table 6).

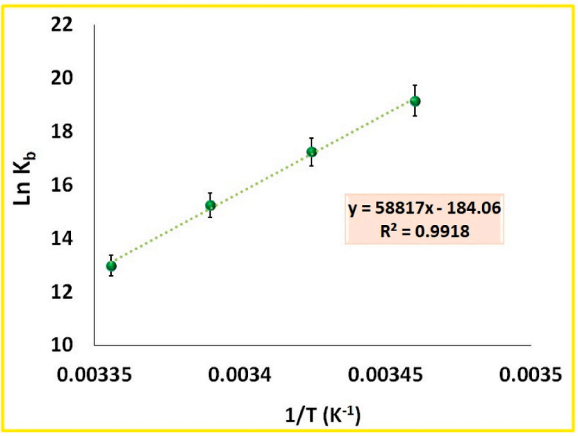

Fig. 6. Straight van't Hoff diagram of the nano-[Cu_2-$(DIP)_2$-EA]-albumin binding.

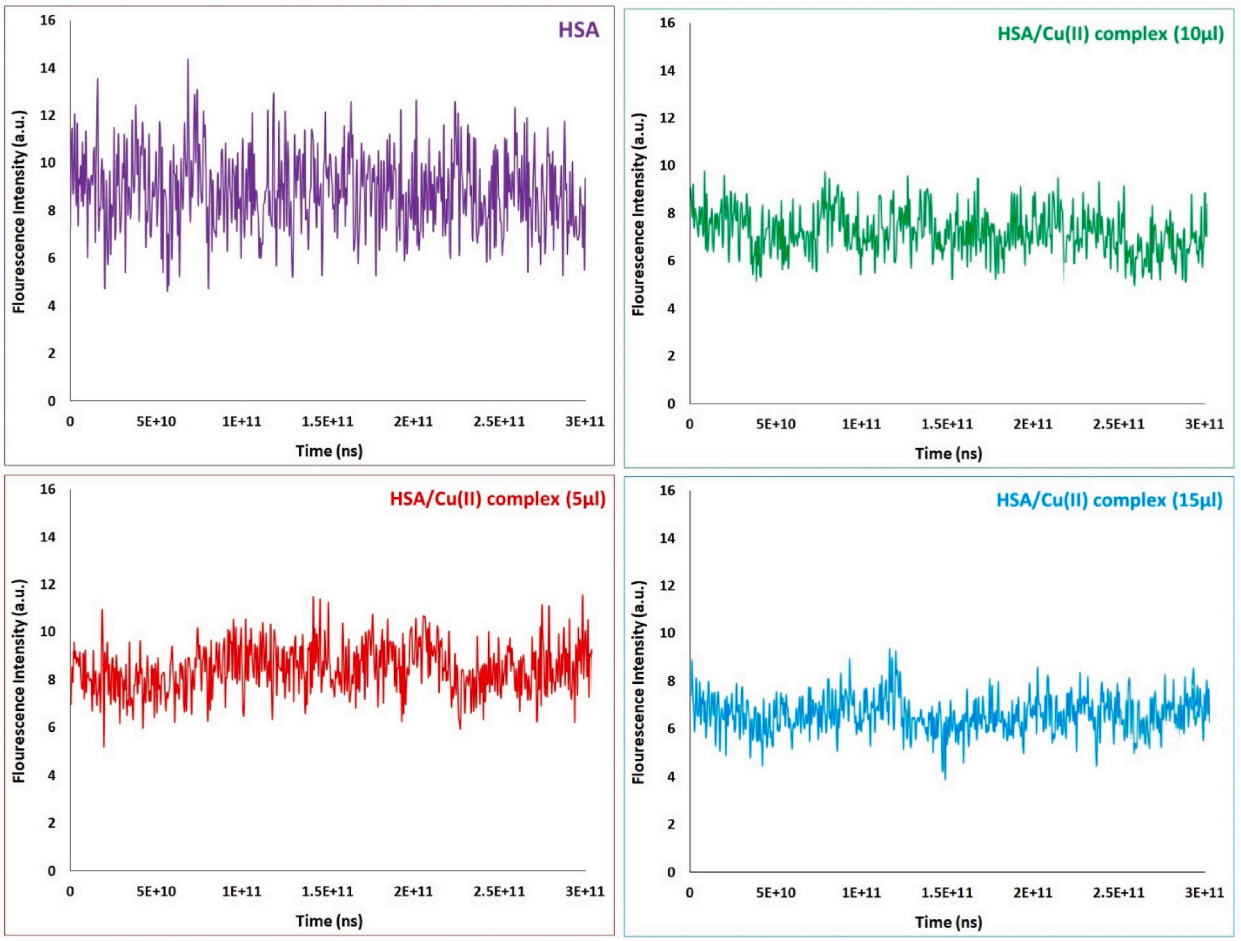

Fig. 7. Time-resolved fluorescence decays for HSA (2.9×10^{-6} M) without and with the concentrations of nano-[Cu_2-$(DIP)_2$-EA] (2.5, 4.9, and 7.5 $\times 10^{-7}$ M) at room temperature.

Table 1
The biomolecule quenching rate constant (k_q), and the quenching constant (K_{SV}) of the nano-[Cu_2-$(DIP)_2$-EA] interacting with albumin at four distinct temperatures.

T (K)	K_{SV} (M^{-1}) × 10^{-4}	k_q ($M^{-1}s^{-1}$) × 10^{-12}	R^2
289	96.3810 ± 2.17	96.3810 ± 2.17	0.9886
292	95.8801 ± 2.11	95.8801 ± 2.11	0.9867
295	51.9009 ± 0.22	51.9009 ± 0.22	0.9952
297	10.3787 ± 0.17	10.3787 ± 0.17	0.9903

Table 2
The binding constants (K_b), and the number of binding sites (n) for the nano-[Cu_2-$(DIP)_2$-EA]-albumin in differing temperature.

T (K)	n	Log K_b	K_b (M^{-1}) × 10^{-6}	R^2
289	1.43 ± 0.16	8.3217 ± 0.331	209.749048 ± 37.56	0.9981
292	1.31 ± 0.25	7.665 ± 0.122	46.238102 ± 12.74	0.9957
295	1.27 ± 0.35	7.1703 ± 0.233	6.313933 ± 0.01158	0.9963
297	1.11 ± 0.21	5.6403 ± 0.141	0.436817 ± 0.01188	0.9875

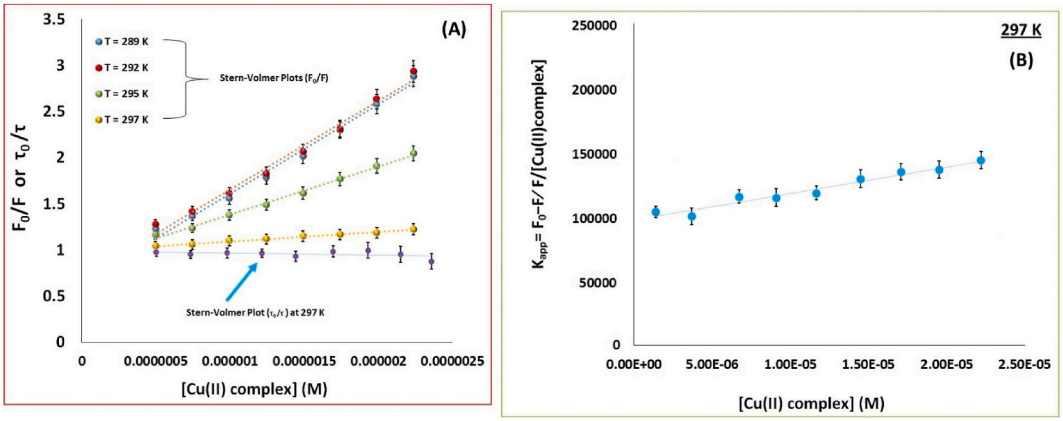

Fig. 8. A) Stern-Volmer plots comparing the steady-state and time-resolved fluorescence data for HSA-nano-[Cu_2-$(DIP)_2$-EA] at 297 K. **B)** The apparent quenching constant plot to the separation of the dynamic and static quenching constants at 297 K.

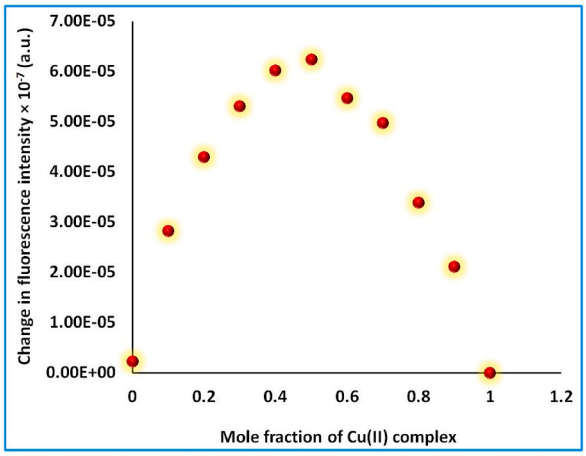

Fig. 9. Job's curve of the nano-[Cu_2-$(DIP)_2$-EA]-protein fluorescence in phosphate buffer; overall concentration ($T_o = 5.0 \times 10^{-6}$ M); excited at 295 nm and 25 °C; pH 7.4.

Table 3
Thermodynamic amounts of the nano-[Cu_2-$(DIP)_2$-EA]-protein adduct in four variant temperature conditions.

T (K)	ΔG (kJ mol^{-1})	ΔH (kJ mol^{-1})	ΔS (J mol^{-1} K^{-1})
289	−46.07 ± 1.61	−489.03 ± 31.47	−1530.36 ± 156.12
292	−42.87 ± 1.34		
295	−36.81 ± 1.22		
297	−32.20 ± 1.13		

Table 4
Comparative evaluation of the binding constant for the nano-[Cu_2-$(DIP)_2$-EA]-albumin system with and without the use of the site tracers at pH 7.4.

T (K)	Adduct	K_b (M^{-1}) × 10^{-4}	R^2
298	nano-[Cu_2-$(DIP)_2$-EA]-HSA	33.7753 ± 2.12	0.9933
	nano-[Cu_2-$(DIP)_2$-EA]-War-HSA	3.9502 ± 0.42	0.9820
	nano-[Cu_2-$(DIP)_2$-EA]-Ibu-HSA	28.5001 ± 1.87	0.9883

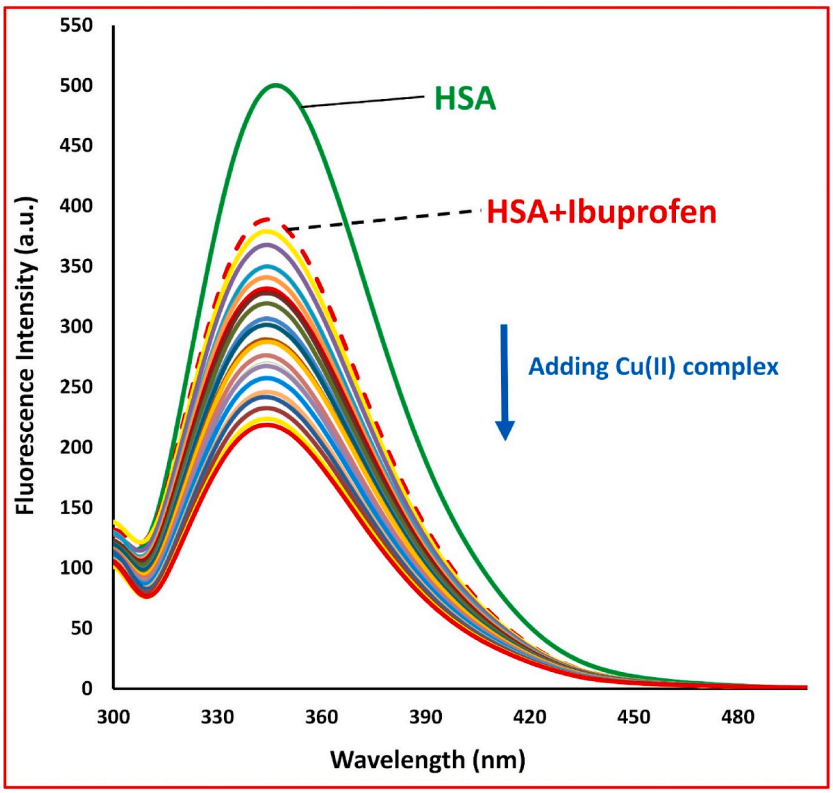

Fig. 10. The nano-[Cu_2-$(DIP)_2$-EA] impact in the ibuprofen-albumin fluorescence into phosphate buffer, excitation = 295 nm [Albumin] = 2.9 × 10^{-6} M, [site tracer] = 2.8 × 10^{-5} M and [nano-[Cu_2-$(DIP)_2$-EA]]: (0.00, 4.71 × 10^{-7} to 8.22 × 10^{-5} M); pH 7.4; 298 K.

Table 5
α-Helix content of serum albumin before and after the addition of nano-[Cu_2-$(DIP)_2$-EA]; 298 K; pH 7.4.

Concentration of nano-[Cu_2-$(DIP)_2$-EA]	α-Helical % (208 nm)
0.00 × 10^{-9} M	66.43 ± 0.232
2.48 × 10^{-9} M	62.58 ± 0.204
4.95 × 10^{-9} M	61.31 ± 0.112
7.41 × 10^{-9} M	55.85 ± 0.147

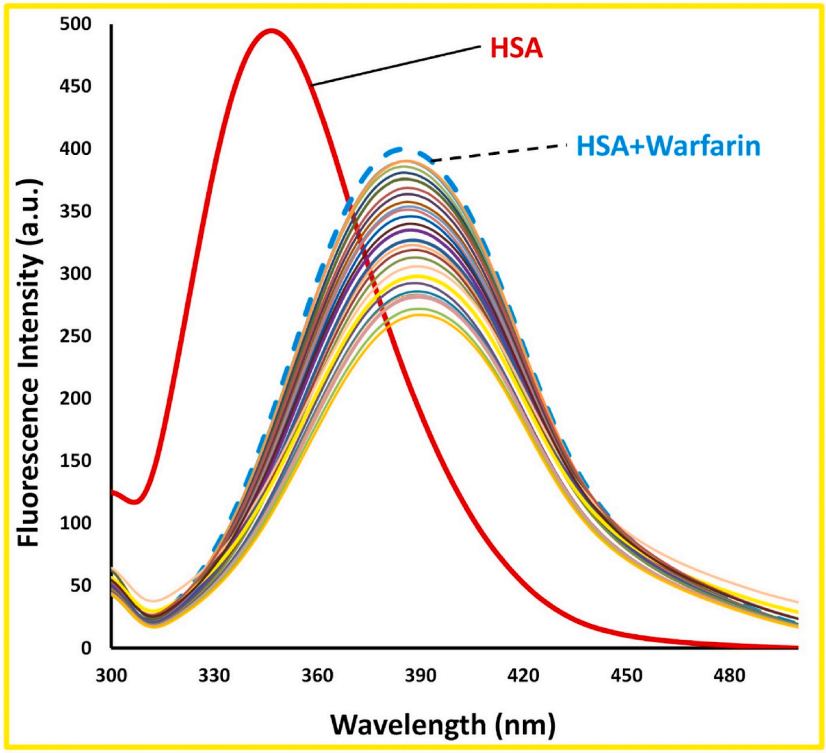

Fig. 11. The nano-[Cu_2-$(DIP)_2$-EA] impact in the warfarin-albumin fluorescence into phosphate buffer, excitation = 295 nm [Albumin] = 2.9×10^{-6} M, [site tracer] = 2.8×10^{-5} M and [nano-[Cu_2-$(DIP)_2$-EA]]: (0.00, 4.71×10^{-7} to 8.22×10^{-5} M); pH 7.4; 298 K.

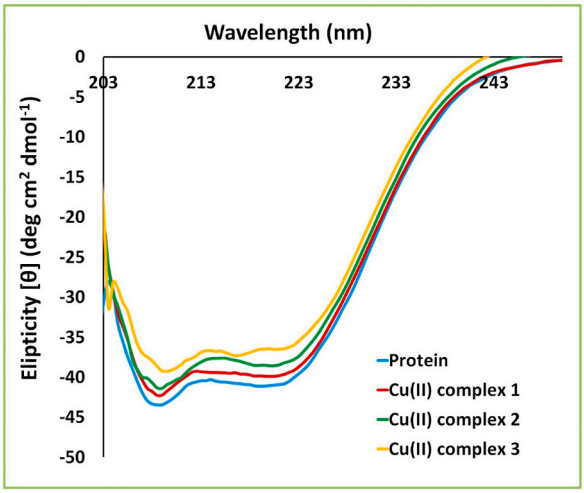

Fig. 12. The CD bands of the serum protein in the non-existence and existence of the nano-[Cu_2-$(DIP)_2$-EA]; [protein] = 4.97×10^{-7} M, [nano-[Cu_2-$(DIP)_2$-EA]] = 0.00, 2.48, 4.95, and 7.41×10^{-9} M; 298K; pH 7.4.

2.10. Data preparation and transformation procedures

2.10.1. UV–vis spectrophotometry

The absorbance data obtained from the UV–Vis spectrophotometer were directly utilized for analysis. Data preparation involved recording absorbance values at varying concentrations of nano-[Cu_2-$(DIP)_2$-EA] relative to HSA.

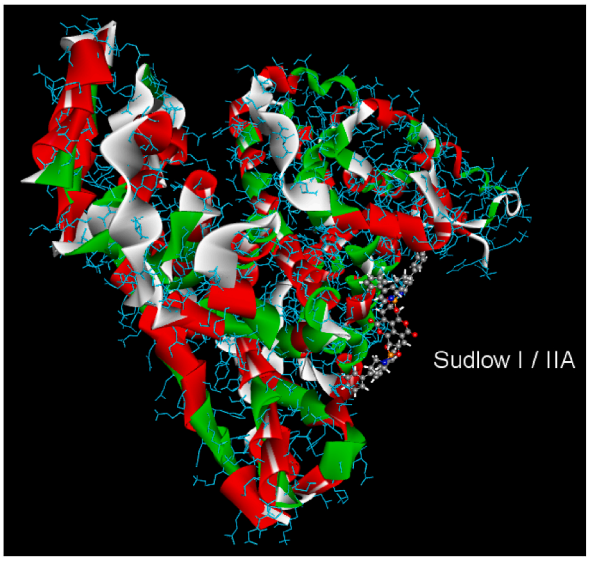

Fig. 13. Structure of HSA and nano-[Cu_2-$(DIP)_2$-EA], illustrating domain IIA and the subdomain of the interaction site I.

Table 6
Docking outcomes for the nano-[Cu_2-$(DIP)_2$-EA]-HSA pattern.

mode	Affinity kcal/mol	dist from rmsd l.b.	best mode rmsd u.b.
1	−10.9	0.000	0.000
2	−10.1	4.843	15.367
3	−9.6	4.715	7.235
4	−9.6	2.597	16.049
5	−9.4	4.361	17.182
6	−9.1	2.659	2.620
7	−8.5	2.158	18.971
8	−8.5	3.479	16.283
9	−8.5	4.607	6.524

2.10.2. Fluorescence spectroscopy

Data preparation included acquiring fluorescence spectra at different temperatures and wavelengths, as well as various concentrations of nano-[Cu_2-$(DIP)_2$-EA] and HSA. Additionally, evaluations of displacement were conducted using specific site markers. Fluorescence intensities were corrected for factors such as the absorption of the excitation light beam and the re-absorption of emitted light using a designated equation (Eq. (1)).

2.10.3. Circular dichroism (CD) Spectropolarimetry

The data preparation for CD involved collecting spectra at different wavelengths and protein concentrations. The data were subsequently converted to mean residual ellipticity utilizing equation (Eq. (7)). Furthermore, the percentage of α-helix content in HSA was calculated based on equation (Eq. (8)), particularly at 208 nm.

2.10.4. Molecular docking

The molecular docking data preparation process entailed acquiring the necessary files for docking. The crystalline form of the protein was sourced from the Protein Data Bank (PDB ID: 7VR0), while the ligand (nano-[Cu_2-$(DIP)_2$-EA]) and receptor (HSA) files were generated using AutoDock Tools. Specific parameters for the grid box, such as dimensions and grid spacing, were established for the docking procedure. The Lamarckian genetic algorithm was employed to define the docking parameters, while default settings were maintained for all other factors. Finally, the docked poses were visualized using BIOVIA Discovery Studio Visualizer 2021.

2.11. Information on the software and versions used for analysis

2.11.1. UV–vis spectrophotometry

UVWin 5.0.

2.11.2. Fluorescence spectroscopy
Spectra Manager II Version 2.2.

2.11.3. Circular dichroism (CD) Spectropolarimetry
JASCO 32-bit Spectra Manager.

2.11.4. Molecular docking
Software previously mentioned.

3. Results and discussion

In this study, we primarily focused on the free concentrations of the nano-[Cu_2-$(DIP)_2$-EA] interacting with HSA. This focus aligns with our hypothesis regarding the effects of these free species on binding dynamics with HSA, allowing us to elucidate the pharmacokinetic implications of these interactions. While we acknowledge that the bound concentrations are significant, we plan to explore this aspect in future studies for a more comprehensive perception of the interactions at play.

3.1. Assessment of nano-[Cu_2-$(DIP)_2$-EA]-HSA interaction in the UV–vis region

The interaction between biomolecules and small molecules, including ligands, often induces significant alterations in UV–visible absorption profiles, indicative of complex formation [41]. UV–visible absorption spectroscopy is a widely utilized technique for investigating structural modifications and the formation of complexes involving biomacromolecules, such as transport proteins like (HSA), along with other molecules [42,43]. This method is particularly favored due to the capability of aromatic amino acid residues within protein structures to absorb ultraviolet light [43]. Consequently, UV–visible spectroscopy can be regarded as a straightforward yet powerful approach for examining the structural changes that occur when the substances under investigation interact to form complexes with HSA [44].

In the UV–visible spectrum of HSA solutions, distinct absorbance peaks are observed at approximately 210 nm and within the range of 275–280 nm, corresponding to $\pi\rightarrow\pi^*$ and $n\rightarrow\pi^*$ transitions, respectively. The absorbance peak at 210 nm is primarily associated with the carbonyl groups present in the peptide bonds of the protein. In contrast, the absorbance between 275 and 280 nm is attributed to the presence of aromatic amino acid residues, including tryptophan (Trp), tyrosine (Tyr), and phenylalanine (Phe). These transitions mirror the inherent structural characteristics of HSA and provide nuanced insights into its biochemical properties [42,43,45,46]. Conformational alterations in the HSA structure are closely linked to the polarity of the microenvironments surrounding amino acid residues, backed by shifts in emission or alterations in the absorption characteristics of these residues [47]. The interaction mechanisms between small compounds and biomacromolecules can be categorized as dynamic or static. Dynamic interactions primarily influence the excited state of fluorophores without modifying the absorption spectrum, whereas static interactions result in observable changes in absorption characteristics due to the formation of stable complexes [42,46].

To investigate the interaction between HSA and nano-[Cu_2-$(DIP)_2$-EA], the absorption band in the range of 275–280 nm was selected. Remarkably, the albumin absorption peak at 278 nm progressively increased upon the addition of nano-[Cu_2-$(DIP)_2$-EA], as illustrated in Fig. 2. The observed hyperchromism and accompanying wavelength shift suggest a robust interaction between nano-[Cu_2-$(DIP)_2$-EA] and the hydrophobic regions of the protein. These spectral changes imply modifications in hydrophobicity, resultant from variations in the polarity surrounding the tryptophan residue. Our appraisals signal that the interaction with nano-[Cu_2-$(DIP)_2$-EA] induces conformational changes and structural adjustments in the HSA molecule, substantiated by the increased absorbance at 278 nm and the consequent exposure of chromophores responsible for absorption at these wavelengths. These alterations likely arise from changes in the local microenvironment surrounding the aromatic residues, along with partial unfolding of the HSA backbone. Furthermore, the binding of nano-[Cu_2-$(DIP)_2$-EA] to HSA appears to proceed via a static quenching mechanism, with minimal perturbation of the microenvironment surrounding the albumin crystallized aromatic amino acid residues [41,42,44,46,48].

The hyperchromism observed in the interaction between nano-[Cu_2-$(DIP)_2$-EA] and HSA is consistent with outcomes derived from multiple studies in the literature. For instance, Liu et al. [49] reported increased absorbance at similar wavelengths connected with the binding of a binuclear Cu(II) complex to bovine serum albumin (BSA), reflecting consistent spectroscopic behavior. Additionally, Peng et al. [50] underscored hyperchromic effects in HSA linked to the binding of various metal complexes, including a Cu(II) complex containing 1,10-phenanthroline ligands, paralleling our observations in the present study. Moreover, Inci et al. [51] detailed the occurrence of static mechanisms and hyperchromic effects in the interaction of two synthesized Cu(II) complexes containing 1, 10-bathophenanthroline ligands with HSA/BSA. Similar results were also reported by Yilmaz et al. [52].

3.2. Fluorimetric investigations of HSA with nano-[Cu_2-$(DIP)_2$-EA]

Steady-state spectrofluorimetry is a broadly adopted technique for elucidating the binding characteristics between biomacromolecules and various compounds [42]. Fluorescence arises from photon emission as an electron transitions from a higher-energy orbital to a lower-energy orbital [48]. This spectroscopic approach is specifically effective in studying protein interactions, owing to the intrinsic fluorescence properties of certain amino acids, especially tryptophan and tyrosine, when incorporated into protein structures. Within the context of HSA, tryptophan, located in subdomain IIA, serves as the predominant contributor to fluorescence emission, while the role of tyrosine is comparatively minor. Both amino acids exhibit fluorescence emission at 315 nm and

340 nm, respectively, upon excitation at 280 nm; however, tryptophan emission can be distinctly observed by exciting HSA at 295 nm [41,42,44,46,48,53,54]. Consequently, tryptophan is frequently employed as a fluorescent probe to explore the interaction dynamics between HSA and various ligands [43]. The binding of a drug or ligand to HSA can induce alterations or quenching of its fluorescence features, propelled by changes in the microenvironment surrounding the fluorescent residue [46,48]. Therefore, spectrofluorimetry was chosen to examine the nature of the nano-[Cu_2-$(DIP)_2$-EA]-HSA interaction due to its simplicity, accuracy, and reliability [46].

The fluorescence emission spectra of albumin at pH 7.4 under varying concentrations of nano-[Cu_2-$(DIP)_2$-EA] at 285, 290, and 298 K are illustrated in Fig. 3A. The intrinsic fluorescence of albumin is characterized by a pronounced peak at approximately 350 nm. While the microenvironment of tryptophan remains predominantly stable, there is a consistent reduction in fluorescence intensity with increasing concentrations of nano-[Cu_2-$(DIP)_2$-EA], accompanied by no significant shifts in the emission peak. This observation denotes that nano-[Cu_2-$(DIP)_2$-EA] binds to albumin, leading to a decrease in its intrinsic fluorescence intensity. Fig. 3B displays the emission spectrum of nano-[Cu_2-$(DIP)_2$-EA], showing a maximum at $\lambda_{max} = 460$ nm when excited at 363 nm.

In fluorescence quenching studies, researchers typically focus on two primary mechanisms: static quenching, which involves the formation of a non-emissive ground-state complex, and dynamic quenching, which occurs when the fluorophore and quencher collide in the excited state. Fluorescence quenching is significantly influenced by temperature, facilitating the assessment of the dominant quenching mechanism. In the case of static quenching, the Stern-Volmer constant (K_{SV}) values decrease with increasing temperature, while the opposite trend is observed for dynamic quenching. The maximum quenching constant in dynamic scenarios involving biomolecules and quenchers averages around 10^{-10} $M^{-1}s^{-1}$ [55]. As shown in Fig. 4, the plots derived from the Stern-Volmer equation for albumin in the presence of escalating concentrations of nano-[Cu_2-$(DIP)_2$-EA] at various temperatures reveal a linear correlation. This finding suggests that the interaction between albumin and nano-[Cu_2-$(DIP)_2$-EA] is chiefly directed by a static quenching mechanism. By analyzing the slope in the regression plot of F_0/F versus [Q], the quenching constants (K_q) and K_{SV} values were calculated (Table 1). The data in Table 1 validate that with rising temperatures, both K_{SV} and K_q values experience a decline. In addition, the computed K_q values exceed 10^{-10} $M^{-1}s^{-1}$, confirming that the quenching process of albumin by nano-[Cu_2-$(DIP)_2$-EA] is indeed static. To derive the binding constant (K_b) and the number of binding sites (n) for small ligands bound to a protein, a double logarithmic analysis can be employed (Eq. (3)). The plot of log $(F_0\text{-}F)/F$ against log [Q] at four distinguished temperatures (Fig. 5) demonstrates a linear relationship, with the slope corresponding to the number of binding sites (n) and the intercept suggestive of the binding constant (K_b). Table 2 summarizes these findings, illustrating the binding affinity of nano-[Cu_2-$(DIP)_2$-EA] to albumin and the presence of a singular binding site. The data in Table 2 uncover that the binding constant for the nano-[Cu_2-$(DIP)_2$-EA]-albumin complex decreases with rising temperature, suggesting a reduction in system stability associated with increased temperature [56]. In essence, the fluorescence quenching of albumin by nano-[Cu_2-$(DIP)_2$-EA] across multiple temperatures detects that the stability of the HSA-nano-[Cu_2-$(DIP)_2$-EA] complex is inversely influenced by temperature. This observation further substantiates the notion that nano-[Cu_2-$(DIP)_2$-EA] induces static quenching of albumin, in agreement with the existing literature [57–60].

Thermodynamic assays constitute a classic methodology employed to elucidate the forces influencing protein-ligand interactions, as proposed by Ross [61]. These experiments utilize thermodynamic parameters (ΔG, ΔS, and ΔH) to evaluate the interactions that transpire between small molecules and larger biological macromolecules. The forces involved commonly encompass hydrophobic interactions ($\Delta H > 0$, $\Delta S > 0$), electrostatic forces ($\Delta H < 0$, $\Delta S > 0$), van der Waals interactions, and hydrogen bonding ($\Delta S < 0$, $\Delta H < 0$), all of which are regarded as weak interactions. A negative ΔG signals the spontaneity of the interaction process [56,61–63]. The thermodynamic parameters, outlined in Table 3 and depicted in Fig. 6, were calculated using equations (Eqs. (4) and (5)). The negative values for ΔG, ΔS, and ΔH imply that the binding of nano-[Cu_2-$(DIP)_2$-EA] to the protein occurs spontaneously, with van der Waals forces and hydrogen bonding identified as the primary driving mechanisms in this interaction [38,64,65]. When comparing these results with appraisals documented in the literature [59,66–68], it is evident that the interaction of various copper complexes with serum albumin proteins is significantly affected by van der Waals forces and hydrogen bonds.

The highly negative ΔH value marks a highly favorable interaction between HSA and nano-[Cu_2-$(DIP)_2$-EA], attributable to robust binding forces, potential cooperative effects, beneficial changes in entropy, and precise measurement methodologies. Collectively, these factors likely contribute to the substantial heat release observed during the interaction. In the studies conducted by Shiri et al. and Shahabadi et al., ΔH values were reported as -304.6 kJ mol^{-1} and -167.768 kJ mol^{-1}, respectively [69,70].

The examination of lifetime measurements aims to further clarify the quenching mechanism at play. Given its inherent sensitivity to interactions within the excited state, fluorescence lifetime measurements have long been recognized as a valuable tool for investigating the microenvironment surrounding fluorophores [36]. So, to deepen the cognition of the fluorescence quenching mechanism in the HSA-nano-[Cu_2-$(DIP)_2$-EA] complex, time-resolved fluorescence measurements were conducted both in the absence and presence of varying concentrations of nano-[Cu_2-$(DIP)_2$-EA], corresponding to those utilized in the steady-state fluorescence analysis (Fig. 7) [27]. Fig. 8 A presents a comparative analysis of Stern-Volmer plots for F_0/F and τ_0/τ at ambient temperature alongside the time-resolved parameters. By applying equations (Eqs. (6)–(8)) and constructing the relevant plots, we determined the static and dynamic quenching constants, $K_D = 7.214 \times 10^3$ M^{-1} and $K_S = 9.2788 \times 10^4$ M^{-1}, respectively. The results signifies that the static quenching constant surpasses the dynamic quenching constant (Fig. 8B), implying that static quenching predominates over dynamic quenching [35]. Moreover, the fluorescence lifetimes for HSA remained relatively stable in the presence of nano-[Cu_2-$(DIP)_2$-EA]. The Stern-Volmer plots for both fluorescence intensities (F_0/F) and lifetimes (τ_0/τ) exhibited linearity, with τ_0/τ approximately equal to one (Fig. 8). These observations suggest that the quenching process primarily operates via a static mechanism, thereby corroborating the results obtained from the steady-state fluorescence measurements [26,27,71,72].

Job's graph evaluation was undertaken to validate the binding affinity of the nano-[Cu_2-$(DIP)_2$-EA]-HSA adduct. The outcomes provided evidence that the fluorescence intensity peaked at a mole fraction of 0.5 for nano-[Cu_2-$(DIP)_2$-EA], implying a 1:1 stoichiometry complexation for nano-[Cu_2-$(DIP)_2$-EA] with HSA. During the experiment, fluorescence emission bands were recorded for a

range of solutions at 298 K, with varying concentrations of HSA and nano-[Cu_2-$(DIP)_2$-EA] while maintaining a constant total concentration (5.0×10^{-6} M). Plotting the fluorescence intensity variations (ΔF) versus the mole fraction of nano-[Cu_2-$(DIP)_2$-EA] was done and the Job's plot breakpoint ascertained the binding stoichiometry of nano-[Cu_2-$(DIP)_2$-EA]-HSA. The binding ratio of 1:1 was specified with the help of the equation (Eq. (9)). Fig. 9 makes prominent a clear break in the fluorescence intensity at the mole fraction = 0.5, reflecting a 1:1 stoichiometric ratio on the nano-[Cu_2-$(DIP)_2$-EA]-HSA compound. Therefore, it can be concluded that only one of HSA's binding sites gets utilized by nano-[Cu_2-$(DIP)_2$-EA] to bind to it [73,74].

Ligand sites 1 and 2, which are the chief binding sites in albumin for drugs found in subdomains IIA and IIIA, respectively, were previously introduced. Ibuprofen binding to ligand site 2 and warfarin binding to ligand site 1 were reported by Ghuman and colleagues. Competitive emission studies were conducted making use of warfarin as a tracer for drug site 1 and ibuprofen as a tracer for drug site 2, bearing in mind the known drug-binding sites. These tracers were deployed to explore the fluorescence quenching of albumin via nano-[Cu_2-$(DIP)_2$-EA], with the corresponding spectra presented in Figs. 10 and 11. The existence of warfarin significantly reduces the binding constant (Table 4). This decrease is attributed to the competition between nano-[Cu_2-$(DIP)_2$-EA] and warfarin for the identical binding site, leading to a lower affinity for the latter. The concentration of ibuprofen, on the other hand, has minimal impact on the HSA binding and nano-[Cu_2-$(DIP)_2$-EA] as shown in Table 4. These results offer that ibuprofen does not affect the nano-[Cu_2-$(DIP)_2$-EA]-protein binding, proposing that the binding site of nano-[Cu_2-$(DIP)_2$-EA] within the protein corresponds to the site where warfarin binds, known as drug site 1 [41,59,65,75]. Literature confirms that other copper complexes and coordination compounds may interact with albumin proteins at site I, as revealed by warfarin tracer [59,69,76,77].

3.3. Circular dichroism analysis

The circular dichroism (CD) technique is based on chirality and provides a clarification of the overall conformation and arrangement of a system [78]. Upon examination of the CD spectra, two conspicuous negative peaks are observed at approximately 208 nm and 222 nm. These peaks arise from specific transitions of $\pi \rightarrow \pi^*$ and $n \rightarrow \pi^*$, respectively, which are attributed to the peptide bonds found in native α-helical proteins [47,79–81].

To assay any changes in the conformation of HSA elicited by nano-[Cu_2-$(DIP)_2$-EA], the CD bands of HSA were analyzed both in the presence and absence of this compound. Mean residual ellipticity (MRE) at 208 nm and the α-helical content of the albumin were calculated using equations (Eqs. (10) and (11)). The analysis presented in Fig. 12 entails that HSA mainly adopts an α-helical conformation, backed by the most negative values at 208 nm and 222 nm. Although the negative ellipticities at these wavelengths remained following the addition of nano-[Cu_2-$(DIP)_2$-EA] to HSA, the intensity of the spectra diminished, suggesting a reduction in α-helical content. Specifically, the protein exhibits a 66.43 % α-helical structure, which decreases to 55.85 % upon the introduction of nano-[Cu_2-$(DIP)_2$-EA] (Table 5).

In summary, the impact of nano-[Cu_2-$(DIP)_2$-EA] on HSA designates an interaction with the protein, leading to alterations in the secondary structure of albumin through a decrease in the helical percentage, while overall stability of the α-helix is maintained. Moreover, the discoveries of this study conform to literature reports on other copper complexes [82–85].

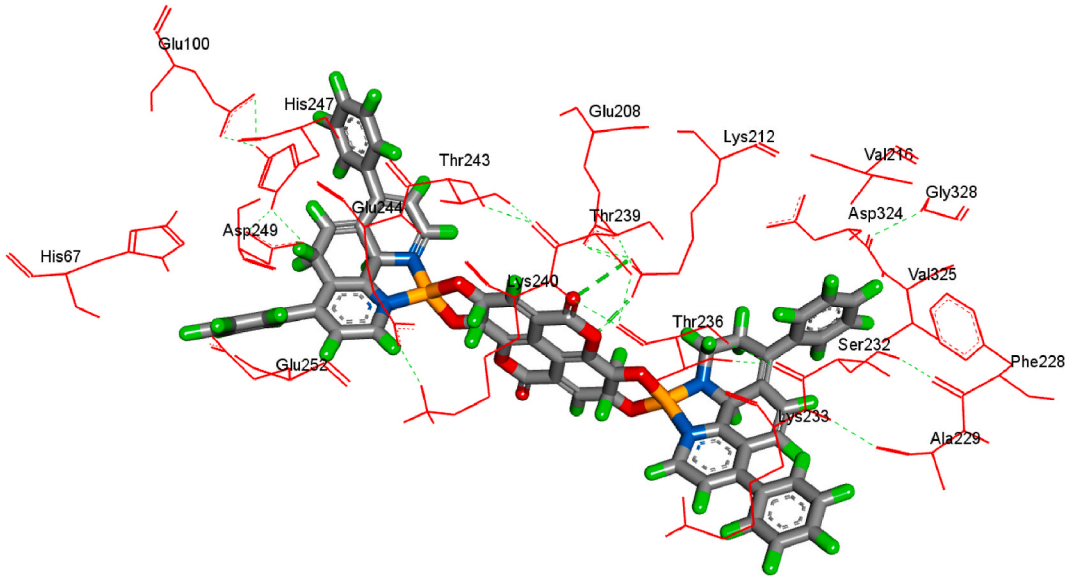

Fig. 14. Close-up view of the amino acids in proximity to nano-[Cu_2-$(DIP)_2$-EA].

3.4. Simulations of molecular docking theory

Molecular modeling theory provides a powerful framework for apprehension the interactions between small molecules and macromolecules. Molecular docking visualization is primarily utilized to model the binding modes of molecules and evaluate the interaction energy [86]. In this study, the interaction mode of nano-[Cu_2-$(DIP)_2$-EA] with serum albumin was predicted through docking simulation analysis. The research indicates that the Sudlow I/IIA site—a well-characterized binding site for drugs and metal complexes—is where nano-[Cu_2-$(DIP)_2$-EA] associates with HSA (Fig. 13). This selected docking position aligns with the region characteristically occupied by warfarin (I-IIA). A detailed exploration of the interactions between adjacent amino acids at the binding site and nano-[Cu_2-$(DIP)_2$-EA] was conducted to verify the proposed binding mode (Fig. 14). The analysis discloses that the HZ1 atom of amino acid Lys 212 forms a hydrogen bond measuring 2.97 Å with the oxygen atom from the carbonyl group of the Cu(II) complex. Furthermore, a second hydrogen bond of 2.18 Å in length is established between the HZ2 atom of the same amino acid and the oxygen atom adjacent to the Cu(II) complex's carbonyl group (Fig. 15). According to Table 6, the scoring function predicts an affinity of approximately −10.9 kcal/mol with an RMSD of 0, suggesting a good correlation between the predicted binding mode and experimental results. These conclusions are consistent with thermodynamic studies conducted in the experimental section ($\Delta H < 0$, $\Delta S < 0$, and $\Delta G < 0$).

4. Conclusion

This study elucidates the interactions between nano-[Cu_2-$(DIP)_2$-EA] and HSA through a comprehensive approach, utilizing fluorescence quenching, UV–visible absorption analysis, and molecular docking calculations. The significant increase in HSA absorption peaks upon successive additions of nano-[Cu_2-$(DIP)_2$-EA] provides strong evidence for molecular binding. The interaction mechanism was identified as the formation of a static complex based on time-resolved fluorescence decay analysis and the temperature dependence of the computed K_{sv} and K_q values. A robust binding affinity ($K_b = 0.33 \times 10^{-6}$ M) was determined for the interaction system, alongside a binding stoichiometry of 1:1. Thermodynamic analyses suggest that hydrogen bonds and van der Waals forces overwhelmingly govern the spontaneous and exothermic binding of nano-[Cu_2-$(DIP)_2$-EA] to the protein. The binding of nano-[Cu_2-$(DIP)_2$-EA] to the HSA site 1/IIA was confirmed through site marker displacement studies. Additionally, the minor perturbation in HSA's secondary structure following interaction with nano-[Cu_2-$(DIP)_2$-EA], as shown by a reduction in α-helical content, highlights the minimal structural changes associated with the binding event. Overall, the findings, supported by molecular docking simulations, provide an in-depth knowledge of the specific binding site (1/IIA) on HSA and illuminate the molecular mechanisms underlying the nano-[Cu_2-$(DIP)_2$-EA]-HSA interaction.

Pronouncement of interest conflict

The authors announce that there is no conflict of interest.

Data availability statement

All data associated with this study have been deposited in the Social Science Research Network (SSRN) and are publicly accessible at https://doi.org/10.2139/ssrn.4835514. If additional details or specific queries arise, readers are encouraged to contact the authors directly.

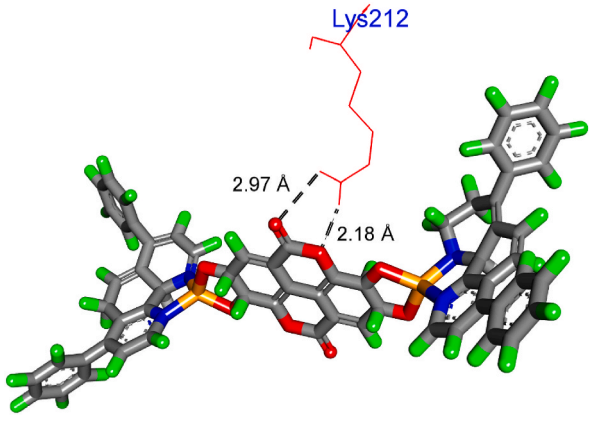

Fig. 15. H-bond interactions between nano-[Cu_2-$(DIP)_2$-EA] and amino acid Lys 212.

CRediT authorship contribution statement

Nahid Shahabadi: Conceptualization. **Lida Ghaffari:** Formal analysis.

Declaration of competing interest

The authors declare that they have no known competing financial interests or personal relationships that could have appeared to influence the work reported in this paper.

Acknowledgments

The authors are aspiring to express their sincere gratitude to the Research Center of Razi University of Kermanshah for financing this work.

References

[1] P. Molaei, H. Mahaki, H. Manoochehri, H. Tanzadehpanah, Binding sites of anticancer drugs on human serum albumin (HSA): a review, Protein Pept, Lett. 29 (2022) 651–675, https://doi.org/10.2174/0929866529666220426124834.
[2] A. Karimipour, A. Karimipour, N.A. Jolfaei, M. Hekmatifar, D. Toghraie, R. Sabetvand, S. Rostami, Prediction of the interaction between HIV viruses and human serum albumin (HSA) molecules using an equilibrium dynamics simulation program for application in biomedical science, J. Mol. Liq. 318 (2020) 113989, https://doi.org/10.1016/j.molliq.2020.113989.
[3] S. Wang, S. Liu, Y. Zhang, J. He, D.H. Coy, L. Sun, Human serum albumin (HSA) and its applications as a drug delivery vehicle, Health Sci. J. 14 (2020) 1–8, https://doi.org/10.36648/1791-809X.14.2.698.
[4] J. Delva-Wiley, I. Jahan, R.H. Newman, L. Zhang, M. Dong, Computational analysis of the binding mechanism of GenX and HSA, ACS Omega 6 (2021) 29166–29170, https://doi.org/10.1021/acsomega.1c04592.
[5] F.M. Valojerdi, A. Farasat, H. Shariatifar, N. Gheibi, Study of HSA interactions with arachidonic acid using spectroscopic methods revealing molecular dynamics of HSA-AA interactions, Biomed. Rep 12 (2020) 125–133, https://doi.org/10.3892/br.2019.1270.
[6] H.S. Mohammed, V.D. Tripathi, Medicinal applications of coordination complexes, J. Phys. Conf. Ser. IOP Publishing (2020) 012070, https://doi.org/10.1088/1742-6596/1664/1/012070.
[7] A. Saini, P. Bansal, Quenching studies as important toolkit for exploring binding propensity of metal complexes with serum albumin and DNA (A review), Pharm. Chem. J. 56 (2022) 545–558, https://doi.org/10.1007/s11094-022-02676-1.
[8] O. Krasnovskaya, A. Naumov, D. Guk, P. Gorelkin, A. Erofeev, E. Beloglazkina, A. Majouga, Copper coordination compounds as biologically active agents, Int. J. Mol. Sci. 21 (2020) 3965, https://doi.org/10.3390/ijms21113965.
[9] J. Northcote-Smith, P. Kaur, K. Suntharalingam, A cancer stem cell potent copper (II) complex with a S, N, S-schiff base ligand and bathophenanthroline, Eur. J. Inorg. Chem. 2021 (2021) 1770–1775, https://doi.org/10.1002/ejic.202100125.
[10] Z. Zeng, J. Cai, F. Li, Y. Weng, Q. Huang, H. Yang, Q. Huang, Y. Wei, Synthesis, crystal structures, DNA interactions, and antitumor activity of two new dinuclear copper (II) complexes with thiazole ligand, RSC Adv. 11 (2021) 40040–40050, https://doi.org/10.1039/D1RA05798G.
[11] M.V. Lunagariya, K.P. Thakor, B.N. Waghela, C. Pathak, M.N. Patel, Design, synthesis, pharmacological evaluation and DNA interaction studies of binuclear Pt (II) complexes with pyrazolo [1, 5-a] pyrimidine scaffold, Appl. Organometal. Chem. 32 (2018) e4222, https://doi.org/10.1002/aoc.4222.
[12] A. Srivastava, K. Srivastava, J. Prasad, Electrochemical and spectral studies of binary and mixed-ligand copper(II) and cobalt(II) complexes with 2,6-dipicolinic acid and bathophenanthroline chelating ligand in aqueous medium, Chem. Data Col. 30 (2020) 100568, https://doi.org/10.1016/j.cdc.2020.100568.
[13] A.B. Asha, R. Narain, Nanomaterials properties, in: Polymer Science and Nanotechnology, Elsevier, 2020, pp. 343–359, https://doi.org/10.1016/B978-0-12-816806-6.00015-7.
[14] S.S. Jawoor, S.A. Patil, M. Kumbar, P.B. Ramawadgi, Green synthesis of nano sized transition metal complexes containing heterocyclic Schiff base: structural and morphology characterization and bioactivity study, J. Mol. Struct. 1164 (2018) 378–385, https://doi.org/10.1016/j.molstruc.2018.03.084.
[15] J.-H. Choi, H.-J. Hwang, S.W. Shin, J.-W. Choi, S.H. Um, B.-K. Oh, A novel albumin nanocomplex containing both small interfering RNA and gold nanorods for synergetic anticancer therapy, Nanoscale 7 (2015) 9229–9237, https://doi.org/10.1039/C5NR00211G.
[16] M. Mohammadikish, F. Bagheri, Hierarchical crystal growth of copper-salpn nanocomplex: from nanoparticles to microtubes, Monatsh. Chem. 148 (2017) 1393–1401, https://doi.org/10.1007/s00706-017-1935-7.
[17] C.R. Maldonado, L. Salassa, N. Gomez-Blanco, J.C. Mareque-Rivas, Nano-functionalization of metal complexes for molecular imaging and anticancer therapy, Coord. Chem. Rev. 257 (2013) 2668–2688, https://doi.org/10.1016/j.ccr.2013.04.014.
[18] M. Ghazaeian, K. Khorsandi, R. Hosseinzadeh, A. Naderi, H. Abrahamse, Curcumin–silica nanocomplex preparation, hemoglobin and DNA interaction and photocytotoxicity against melanoma cancer cells, J. Biomol. Struct. Dyn. 39 (2021) 6606–6616, https://doi.org/10.1080/07391102.2020.1802342.
[19] J. Sharifi-Rad, C. Quispe, C.M.S. Castillo, R. Caroca, M.A. Lazo-Vélez, H. Antonyak, A. Polishchuk, R. Lysiuk, P. Oliinyk, L. De Masi, Ellagic acid: a review on its natural sources, chemical stability, and therapeutic potential, Oxid. Med. Cell. Longev. 2022 (2022), https://doi.org/10.1155/2022/3848084.
[20] H. Zhu, Y. Yan, Y. Jiang, X. Meng, Ellagic acid and its anti-aging effects on central nervous system, Int. J. Mol. Sci. 23 (2022) 10937, https://doi.org/10.3390/ijms231810937.
[21] G. Zuccari, S. Baldassari, G. Ailuno, F. Turrini, S. Alfei, G. Caviglioli, Formulation strategies to improve oral bioavailability of ellagic acid, Appl. Sci. 10 (2020) 3353, https://doi.org/10.3390/app10103353.
[22] S. Alfei, B. Marengo, G. Zuccari, Oxidative stress, antioxidant capabilities, and bioavailability: ellagic acid or urolithins? Antioxidants 9 (2020) 707, https://doi.org/10.3390/antiox9080707.
[23] A.J. Amor, C. Gómez-Guerrero, E. Ortega, A. Sala-Vila, I. Lázaro, Ellagic acid as a tool to limit the diabetes burden: updated evidence, Antioxidants 9 (2020) 1226, https://doi.org/10.3390/antiox9121226.
[24] N. Shahabadi, L. Ghaffari, L. Soltani, Synthesis, characterization and biological applications of a new nano-sized binuclear copper(II) complex containing bathophenanthroline and ellagic acid as ligands, J. Mol. Struct. 138139 (2024), https://doi.org/10.1016/j.molstruc.2024.138139.
[25] A. Costa-Tuna, O.A. Chaves, R.J. Loureiro, S. Pinto, J. Pina, C. Serpa, Interaction between a water-soluble anionic porphyrin and human serum albumin unexpectedly stimulates the aggregation of the photosensitizer at the surface of the albumin, Int. J. Biol. Macromol. 255 (2024) 128210, https://doi.org/10.1016/j.ijbiomac.2023.128210.
[26] A. Costa-Tuna, O.A. Chaves, Z.L. Almeida, R.S. Cunha, J. Pina, C. Serpa, Profiling the interaction between human serum albumin and clinically relevant HIV reverse transcriptase inhibitors, Viruses 16 (2024) 491, https://doi.org/10.3390/v16040491.
[27] M.A.G. Soares, F. Souza-Silva, C.R. Alves, L. Vazquez, T.S. de Araujo, C. Serpa, O.A. Chaves, Evidence of hyperglycemic levels improving the binding capacity between human serum albumin and the antihypertensive drug hydrochlorothiazide, Sci. Pharm. 92 (2024) 32, https://doi.org/10.3390/scipharm92020032.
[28] A.S. Abdelhameed, A.M. Alanazi, A.H. Bakheit, H.W. Darwish, H.A. Ghabbour, I.A. Darwish, Fluorescence spectroscopic and molecular docking studies of the binding interaction between the new anaplastic lymphoma kinase inhibitor crizotinib and bovine serum albumin, Spectrochim. Acta Mol. Biomol. Spectrosc. 171 (2017) 174–182, https://doi.org/10.1016/j.saa.2016.08.005.

[29] A. Banerjee, M. Mohanty, S. Lima, R. Samanta, E. Garribba, T. Sasamori, R. Dinda, Synthesis, structure and characterization of new dithiocarbazate-based mixed ligand oxidovanadium(IV) complexes: DNA/HSA interaction, cytotoxic activity and DFT studies, New J. Chem. 44 (2020) 10946–10963, https://doi.org/10.1039/D0NJ01246G.
[30] F. Macii, T. Biver, Spectrofluorimetric analysis of the binding of a target molecule to serum albumin: tricky aspects and tips, J. Inorg. Biochem. 216 (2021) 111305, https://doi.org/10.1016/j.jinorgbio.2020.111305.
[31] S. Amézqueta, J.L. Beltrán, A.M. Bolioli, L. Campos-Vicens, F.J. Luque, C. Ràfols, Evaluation of the interactions between human serum albumin (HSA) and non-steroidal anti-inflammatory (NSAIDs) drugs by multiwavelength molecular fluorescence, structural and computational analysis, Pharmaceuticals 14 (2021) 214, https://doi.org/10.3390/ph14030214.
[32] N.C. Bessas, L.A. da Silva, M. Comar Júnior, R.G. de Lima, Interaction of the nitrosyl ruthenium complex [RuII(NH.NHq-R)(tpy)NO]3+ with human serum albumin: a spectroscopic and computational investigation, Luminescence 36 (2021) 391–408, https://doi.org/10.1002/bio.3955.
[33] M.A. Abdelaziz, M. Shaldam, R.A. El-Domany, F. Belal, Multi-spectroscopic, thermodynamic and molecular dynamic simulation studies for investigation of interaction of dapagliflozin with bovine serum albumin, Spectrochim. Acta Mol. Biomol. Spectrosc. 264 (2022) 120298, https://doi.org/10.1016/j.saa.2021.120298.
[34] N. Adam, C. Adam, M. Keskitalo, J. Pfeuffer-Rooschüz, P.J. Panak, Interaction of Cm(III) with human serum albumin studied by time-resolved laser fluorescence spectroscopy and NMR, J. Inorg. Biochem. 192 (2019) 45–51, https://doi.org/10.1016/j.jinorgbio.2018.12.007.
[35] M.D. Meti, K.S. Byadagi, S.T. Nandibewoor, S.D. Joshi, U.A. More, S.A. Chimatadar, In vitro studies on the interaction between human serum albumin and fosfomycin disodium salt, an antibiotic drug by multi-spectroscopic and molecular docking methods, Mol. Biol. Rep. 41 (2014) 2377–2387, https://doi.org/10.1007/s11033-014-3092-y.
[36] M.D. Meti, S.T. Nandibewoor, S.D. Joshi, U.A. More, S.A. Chimatadar, Binding interaction and conformational changes of human serum albumin with ranitidine studied by spectroscopic and time-resolved fluorescence methods, J. Iran. Chem. Soc. 13 (2016) 1325–1338, https://doi.org/10.1007/s13738-016-0847-5.
[37] P. Job, Formation and Stability of Inorganic Complexes in Solution, Annales de Chimie, France) 9 (1928) 113–203.
[38] K. Azeem, M. Ahmed, T. Mohammad, A. Uddin, A. Shamsi, M.I. Hassan, S. Singh, R. Patel, M. Abid, A multi-spectroscopic and computational simulations study to delineate the interaction between antimalarial drug hydroxychloroquine and human serum albumin, J. Biomol. Struct. Dyn. 41 (2023) 6377–6393, https://doi.org/10.1080/07391102.2022.2107077.
[39] W. Xiang, Z.L. Yue, J.Y. Su, Human serum albumin. https://doi.org/10.2210/pdb7VR0/pdb, 2022.
[40] D.S. Biovia, Discovery Studio Modeling Environment, Release, 2017.
[41] M.S. Ali, H.A. Al-Lohedan, Experimental and computational investigation on the interaction of anticancer drug gemcitabine with human plasma protein: effect of copresence of ibuprofen on the binding, Molecules 27 (2022) 1635, https://doi.org/10.3390/molecules27051635.
[42] T.V. Acunha, O.A. Chaves, B.A. Iglesias, Fluorescent pyrene moiety in fluorinated C6F5-corroles increases the interaction with HSA and CT-DNA, J. Porphyrins Phthalocyanines 25 (2021) 75–94, https://doi.org/10.1142/S1088424620500534.
[43] M.C. Vlasiou, K.S. Pafiti, Spectroscopic evaluation of Zn(II) complexes with drug analogues: interactions with BSA and the pH effect on the drug-Zn(II) system, Spectrochim. Acta Mol. Biomol. Spectrosc. 241 (2020) 118641, https://doi.org/10.1016/j.saa.2020.118641.
[44] M. Salim, M.E. El Sharkasy, F. Belal, M. Walash, Multi-spectroscopic and molecular docking studies for binding interaction between fluvoxamine and human serum albumin, Spectrochim. Acta Mol. Biomol. Spectrosc. 252 (2021) 119495, https://doi.org/10.1016/j.saa.2021.119495.
[45] M.A. Bratty, Spectroscopic and molecular docking studies for characterizing binding mechanism and conformational changes of human serum albumin upon interaction with telmisartan, Saudi Pharm. J. 28 (2020) 729–736, https://doi.org/10.1016/j.jsps.2020.04.015.
[46] N.A. Alsaif, T.A. Wani, A.H. Bakheit, S. Zargar, Multi-spectroscopic investigation, molecular docking and molecular dynamic simulation of competitive interactions between flavonoids (quercetin and rutin) and sorafenib for binding to human serum albumin, Int. J. Biol. Macromol. 165 (2020) 2451–2461, https://doi.org/10.1016/j.ijbiomac.2020.10.098/.
[47] N. Farajzadeh-Dehkordi, S. Farhadian, Z. Zahraei, N. Gholamian-Dehkordi, B. Shareghi, Interaction of reactive Red 195 with human serum albumin: determination of the binding mechanism and binding site by spectroscopic and molecular modeling methods, J. Mol. Liq. 327 (2021) 114835, https://doi.org/10.1016/j.molliq.2020.114835.
[48] M.S. Ali, J. Muthukumaran, M. Jain, T. Santos-Silva, H.A. Al-Lohedan, N.S. Al-Shuail, Molecular interactions of cefoperazone with bovine serum albumin: extensive experimental and computational investigations, J. Mol. Liq. 337 (2021) 116354, https://doi.org/10.1016/j.molliq.2021.116354.
[49] Y.-F. Liu, X.-Y. Xu, H.-T. Xia, D.-Q. Wang, H. Liu, Synthesis, crystal structure and bovine serum albumin interaction studies of a binuclear copper(II) complex with naphthylacetic acid, Synth. React. Inorg., Met.-Org., Nano-Met. Chem. 39 (2009) 400–405, https://doi.org/10.1080/15533170903129752.
[50] B. Peng, Z. Gao, X. Li, T. Li, G. Chen, M. Zhou, J. Zhang, DNA binding, DNA cleavage and HSA interaction of several metal complexes containing N-(2-hydroxyethyl)-N′-benzoylthiourea and 1,10-phenanthroline ligands, JBIC, J. Biol. Inorg. Chem. 21 (2016) 903–916, https://doi.org/10.1007/s00775-016-1388-1.
[51] D. Inci, R. Aydin, T. Sevgi, Y. Zorlu, E. Demirkan, Synthesis, crystal structure, stability studies, DNA/albumin interactions, and antimicrobial activities of two Cu (II) complexes with amino acids and 5-nitro-1,10-phenanthroline, J. Coord. Chem. 70 (2017) 512–543, https://doi.org/10.1080/00958972.2016.1267729.
[52] V.T. Yilmaz, C. Icsel, F. Suyunova, M. Aygun, N. Aztopal, E. Ulukaya, Ni(II)/Cu(II)/Zn(II) 5,5-diethylbarbiturate complexes with 1,10-phenanthroline and 2,2′-dipyridylamine: synthesis, structures, DNA/BSA binding, nuclease activity, molecular docking, cellular uptake, cytotoxicity and the mode of cell death, Dalton Trans. 45 (2016) 10466–10479, https://doi.org/10.1039/C6DT01726F.
[53] S.U. Parsekar, K. Paliwal, P. Haldar, P.S. Antharjanam, M. Kumar, Synthesis, characterization, crystal structure, DNA and HSA Interactions, and anticancer activity of a mononuclear Cu(II) complex with a Schiff base ligand containing a thiadiazoline moiety, ACS Omega 7 (2022) 2881–2896, https://doi.org/10.1021/acsomega.1c05750.
[54] S. Gurusamy, K. Krishnaveni, M. Sankarganesh, R.N. Asha, A. Mathavan, Synthesis, characterization, DNA interaction, BSA/HSA binding activities of VO(IV), Cu (II), and Zn(II) Schiff base complexes and its molecular docking with biomolecules, J. Mol. Liq. 345 (2022) 117045, https://doi.org/10.1016/j.molliq.2021.117045.
[55] A. Jahanban Esfahlan, L. Roufegarinejad, M. Tabibiazar, J.M. Lorenzo Rodríguez, R. Amarowicz, Exploring the interactions between caffeic acid and human serum albumin using spectroscopic and molecular docking techniques, Polish J. Food Nutr. Sci. (2021). http://hdl.handle.net/11093/3123.
[56] M. Yang, D. Shi, Y. Wang, A.G. Ebadi, M. Toughani, Study on interaction of coomassie brilliant blue G-250 with bovine serum albumin by multispectroscopic, Int. J. Pept. Res. Ther. 27 (2021) 421–431, https://doi.org/10.1007/s10989-020-10096-6.
[57] L. Andrezálová, J. Plšíková, J. Janočková, K. Koňariková, I. Žitňanová, M. Kohútová, M. Kožurková, DNA/BSA binding ability and genotoxic effect of mono- and binuclear copper(II) complexes containing a Schiff base derived from salicylaldehyde and D,L-glutamic acid, J. Organomet. Chem. 827 (2017) 67–77, https://doi.org/10.1016/j.jorganchem.2016.11.007.
[58] Z. Chen, Y. Wu, Z. Zhu, Y. Zhang, DNA cleavage, DNA/HSA binding study, and antiproliferative activity of a phenolate-bridged binuclear copper(II) complex, Biometals 32 (2019) 227–240, https://doi.org/10.1007/s10534-019-00172-w.
[59] S. Hadidi, A binuclear Cu(I)-phosphine complex as a specific HSA site I binder: synthesis, X-ray structure determination, and a comprehensive HSA interaction analysis, J. Biomol. Struct. Dyn. 41 (2023) 7616–7626, https://doi.org/10.1080/07391102.2022.2123401.
[60] X.-W. Li, X.-H. Zhao, Y.-T. Li, Z.-Y. Wu, Synthesis and crystal structure of bicopper(II) complexes: the influence of bridging ligands on DNA/BSA binding behaviors and in vitro antitumor activity, Inorg. Chim. Acta. 488 (2019) 219–228, https://doi.org/10.1016/j.ica.2019.01.026.
[61] P.D. Ross, S. Subramanian, Thermodynamics of protein association reactions: forces contributing to stability, Biochemistry 20 (1981) 3096–3102, https://doi.org/10.1021/bi00514a017.
[62] H. Yang, Q. Zeng, Z. He, D. Wu, H. Li, Interaction of novel Aurora kinase inhibitor MK-0457 with human serum albumin: insights into the dynamic behavior, binding mechanism, conformation and esterase activity of human serum albumin, J. Pharm. Biomed. Anal. 178 (2020) 112962, https://doi.org/10.1016/j.jpba.2019.112962.

[63] Y. Zhang, Y. Cao, Y. Li, X. Zhang, Interactions between human serum albumin and sulfadimethoxine determined using spectroscopy and molecular docking, Molecules 27 (2022) 1526, https://doi.org/10.3390/molecules27051526.
[64] S.-j. Zheng, N. Zheng, M.-l. Zhang, F.-f. Wu, S.-d. Yang, X.-h. Cheng, H.-y. Bao, R. Zhang, Probing the binding mechanism of the verbascoside and human serum albumin by fluorescence spectroscopy and molecular docking approach, Monatshefte für Chemie - Chem. Monthly 154 (2023) 151–158, https://doi.org/10.1007/s00706-022-03002-x.
[65] H. Zhou, Z. Xiong, X. Ma, L. Dai, L. Kuang, R. Deng, X. Lv, X. Tuo, A multispectral study and computer simulation on the interaction of pomalidomide with human serum albumin, J. Mol. Liq. 382 (2023) 121947, https://doi.org/10.1016/j.molliq.2023.121947.
[66] M.Z. Eraj, L. Eriksson, M. Alibolandi, M. Babaei, A.S. Saljooghi, M. Ramezani, Synthesis, X-ray structure, antiproliferative activity, interaction with HSA and docking studies of three novel mono and binuclear copper complexes containing the maltol ligand, New J. Chem. 44 (2020) 20101–20114, https://doi.org/10.1039/D0NJ03552A.
[67] Z. Asadi, M. Golchin, V. Eigner, M. Dusek, Z. Amirghofran, A novel water-soluble tetranuclear copper(II) Schiff base cluster bridged by 2,6-bis-[(2-hydroxyethylimino)methyl]-4-methylphenol in interaction with BSA: synthesis, X-ray crystallography, docking and cytotoxicity studies, J. Photochem. Photobiol., A: Chem 361 (2018) 93–104, https://doi.org/10.1016/j.jphotochem.2018.05.016.
[68] R. Maity, B. Manna, S. Maity, K. Jana, T. Maity, M. Afzal, N. Sepay, B.C. Samanta, Synthesis of an aryl-semicarbazone-based Cu(II) complex for DNA and BSA interaction and anti-cancer activity against human cervix uteri carcinoma, Inorganics 12 (2024) 19, https://doi.org/10.3390/inorganics12010019.
[69] F. Shiri, M. Rahimi-Nasrabadi, F. Ahmadi, H. Ehrlich, Multispectroscopic and molecular modeling studies on the interaction of copper-ibuprofenate complex with bovine serum albumin (BSA), Spectrochim. Acta: Mol. Biomol. Spectrosc. 203 (2018) 510–521, https://doi.org/10.1016/j.saa.2018.05.098.
[70] N. Shahabadi, A. Khorshidi, N.H. Moghadam, Study on the interaction of the epilepsy drug, zonisamide with human serum albumin (HSA) by spectroscopic and molecular docking techniques, Spectrochim. Acta: Mol. Biomol. Spectrosc. 114 (2013) 627–632, https://doi.org/10.1016/j.saa.2013.05.092.
[71] M.A.G. Soares, P.A. de Aquino, T. Costa, C. Serpa, O.A. Chaves, Insights into the effect of glucose on the binding between human serum albumin and the nonsteroidal anti-inflammatory drug nimesulide, Int. J. Biol. Macromol. 265 (2024) 131148, https://doi.org/10.1016/j.ijbiomac.2024.131148.
[72] O.v.A. Chaves, R.J. Loureiro, A. Costa-Tuna, Z.L. Almeida, J. Pina, R.M. Brito, C. Serpa, Interaction of two commercial azobenzene food dyes, amaranth and new coccine, with human serum albumin: biophysical characterization, ACS Food Sci. Technol. 3 (2023) 955–968, https://doi.org/10.1021/acsfoodscitech.3c00125.
[73] J. Zhang, X. Gao, J. Huang, H. Wang, Probing the interaction between human serum albumin and 9-hydroxyphenanthrene: a spectroscopic and molecular docking study, ACS Omega 5 (2020) 16833–16840, https://doi.org/10.1021/acsomega.0c02031.
[74] G.J. Shree, G. Sivaraman, A. Siva, D. Chellappa, Anthracene- and pyrene-bearing imidazoles as turn-on fluorescent chemosensor for aluminum ion in living cells, Dyes Pigments 163 (2019) 204–212, https://doi.org/10.1016/j.dyepig.2018.11.061.
[75] N. Shahabadi, S. Hadidi, Z. Abdoli, Z. Mardani, Interaction of a cobalt(III) complex containing β-amino alcohol with human serum albumin (HSA): spectroscopic and molecular docking methods, J. Mol. Liq. 384 (2023) 122187, https://doi.org/10.1016/j.molliq.2023.122187.
[76] P. Sengupta, U. Pal, P. Mondal, A. Bose, Multi-spectroscopic and computational evaluation on the binding of sinapic acid and its Cu(II) complex with bovine serum albumin, Food Chem. 301 (2019) 125254, https://doi.org/10.1016/j.foodchem.2019.125254.
[77] J. Ruiz, C. Vicente, C. de Haro, D. Bautista, Novel bis-C,N-cyclometalated iridium(III) thiosemicarbazide antitumor complexes: interactions with human serum albumin and DNA, and inhibition of cathepsin B, Inorg. Chem. 52 (2013) 974–982, https://doi.org/10.1021/ic302219v.
[78] A. Kellett, Z. Molphy, C. Slator, V. McKee, N.P. Farrell, Molecular methods for assessment of non-covalent metallodrug–DNA interactions, Chem. Soc. Rev. 48 (2019) 971–988, https://doi.org/10.1039/C8CS00157J.
[79] M.A. Qureshi, S. Javed, Aflatoxin B1 induced structural and conformational changes in bovine serum albumin: a multispectroscopic and circular dichroism-based study, ACS Omega 6 (2021) 18054–18064, https://doi.org/10.1021/acsomega.1c01799.
[80] M. Amir, M.A. Qureshi, S. Javed, Biomolecular interactions and binding dynamics of tyrosine kinase inhibitor erdafitinib, with human serum albumin, J. Biomol. Struct. Dyn. 39 (2021) 3934–3947, https://doi.org/10.1080/07391102.2020.1772880.
[81] S. Lyu, W. Wang, Spectroscopic methodologies and computational simulation studies on the characterization of the interaction between human serum albumin and astragalin, J. Biomol. Struct. Dyn. 39 (2021) 2959–2970, https://doi.org/10.1080/07391102.2020.1758213.
[82] Q. Gan, X. Fu, W. Chen, Y. Xiong, Y. Fu, S. Chen, X. Le, Synthesis, DNA/HSA interaction spectroscopic studies and in vitro cytotoxicity of a new mixed ligand Cu (II) complex, J. Fluoresc. 26 (2016) 905–918, https://doi.org/10.1007/s10895-016-1779-2.
[83] S. Jiang, H. Ni, F. Liu, S. Gu, P. Yu, Y. Gou, Binuclear Schiff base copper(II) complexes: syntheses, crystal structures, HSA interaction and anti-cancer properties, Inorg. Chim. Acta. 499 (2020) 119186, https://doi.org/10.1016/j.ica.2019.119186.
[84] L. Li, Q. Guo, J. Dong, T. Xu, J. Li, DNA binding, DNA cleavage and BSA interaction of a mixed-ligand copper(II) complex with taurine Schiff base and 1,10-phenanthroline, J. Photochem. Photobiol. B Biol. 125 (2013) 56–62, https://doi.org/10.1016/j.jphotobiol.2013.05.007.
[85] S. Tabassum, W.M. Al-Asbahy, M. Afzal, F. Arjmand, Synthesis, characterization and interaction studies of copper based drug with Human Serum Albumin (HSA): spectroscopic and molecular docking investigations, J. Photochem. Photobiol. B Biol. 114 (2012) 132–139, https://doi.org/10.1016/j.jphotobiol.2012.05.021.
[86] N. Alisufi, H. Mansouri-Torshizi, Preparation, characterization, DNA/BSA interaction and computational binding analyses of a dinuclear, biopotency Pd^{2+} coordinated with 1,4-phenylenediamine and ethylenediamine as ligands, J. Iranian Chem. Soc. 18 (2021) 1147–1166, https://doi.org/10.1007/s13738-020-02098-4.